بسم الله الرحمن الرحيم

EXPERIMENTAL AND NUMERICAL MODELLING OF BREAK WATER OVERTOPPING FOR PLAIN, CONVERGING AND STAIRS SLOPE

A thesis submitted to the department of Mechanical and Production Engineering (MPE), Islamic University of Technology (IUT), in the fulfilment of the requirement for degree of Bachelor in Mechanical Engineering.

Prepared By:

Niyaz Afnan Ahmed (160011012)

Maysha Tahsin (160011019)

Supervised By: Dr. M. Hamidur Rahman

Department of Mechanical and Production Engineering

Islamic University of Technology

CERTIFICATE OF RESEARCH:

The thesis title "**Experimental and numerical modelling of break water overtopping for plain, converging and stairs slope**" submitted by **NIYAZ AFNAN AHMED (160011012)** and **MAYSHA TAHSIN(160011019)**, has been accepted as satisfactory in fulfilment of the requirement for the Degree of Bachelor of science in Mechanical and Production Engineering on March, 2021.

Signature of the Supervisor

Rahman 15/03/21

Dr. M. Hamidur Rahman

Professor

Department of Mechanical and Production Engineering

Islamic University of Technology

CANDIDATE DECLARATION

It is hereby declared that this thesis or any part of it has not been submitted elsewhere for the award of any degree.

Signature of the Candidates.

15.03.21

Md. Niyaz Afnan Ahmed

Student ID: 160011012

Maysha Tahsin

15/03/21

Maysha Tahsin

Student ID: 160011019

Department of Mechanical & Production Engineering (MPE)

Islamic University of Technology (IUT), OIC

Board Bazar, Gazipur Bangladesh.

Signature of the Supervisor

Rahman 15/03/21

Dr. M. Hamidur Rahman

Professor

Department of Mechanical & Production Engineering (MPE)

Islamic University of Technology (IUT), OIC

Board Bazar, Gazipur, Bangladesh.

ACKNOWLEDGEMENT:

We would like to begin by saying Alhamdulillah and grateful to Almighty Allah who made it possible for us to finish this work successfully on time. Equally say a big thank you to our supervisor Dr. M. Hamidur Rahman, Professor, Department of Mechanical and Production Engineering, IUT for all his support, ideas about experiments, discussions, time and for explaining so patiently the hard topics and checking this thesis and papers above all his care and concern. These will ever remain in our memory. Thanks to our examiners for their constructive ideas, suggestions and double checking our work.

We seek excuse for any errors that might be in this report despite our best efforts.

ABSTRACT:

In recent years, emphasis has been given on converting wave energies in a stable form to protect coastal areas from erosion. Wave energy has grown to develop the reputation of being a major and promising energy resource which has great potential of being the subject of much research. Wave energy converters have been studied for converting wave energies to stable and useful forms of energy. Numerical wave tanks have performed a remarkable role as a numerical tool for wave converters. The objective of this study is to employ wave tanks both experimentally and numerically. To compound to that, the main aim of this article is to present the characteristics of different types of wave overtopping structures on overtopping discharge. The numerical models have been presented using 3D Navier Stokes solver. Furthermore, Volume of fluid (VOF) method and RANS approach with k-ϵ model has been implemented for treating air-water interfaces and turbulence, respectively. Physical wave tanks with overtopping structures have been physically modelled with experiments carried out for different overtopping structures and the results obtained are then compared. Three different overtopping structure configurations have been studied namely Plain slope, Converging slope and Stairs slope. The overtopping structures have been constructed and the same dimensions used for numerical models. The experimental model has been validated against the numerical one and the accuracy has been verified and they are found to be in reasonable agreement. By generating mesh blocks of different cell numbers, grid independency study was implemented to resolve the perfect mesh size that provides a balance between accuracy and computational time to be used for rest of the simulations. Finally, the performance of the overtopping structures has been carried out for different

frequencies and water levels. Accordingly, the obtained results and comparisons are demonstrated in this paper.

Keywords: Numerical wave tank, overtopping, VOF, wave energy converters

LIST OF FIGURES:

Figure 1 Snapshot of the experimental Model 07

Figure 2 Side view of wave tank with the three shapes: (a) plain slope; (b) converging slope; (c) stairs slope 10

Figure 3 Wave generation in the NWT for three different shapes: (a) plain slope; (b) converging slope; (c) stairs slope 11

Figure 4 Boundary conditions of the numerical wave tank 16

Figure 5 Meshing of geometry: (a) The entire wave tank; (b) Wave maker section and (c) Plain slope section 17

Figure 6 Comparison of flow rate for different cell numbers 19

Figure 7 Pressure contour for plain slope in X-Y plane at different times:(a)10 s; (b) 20 s; (c) 30 s 21

Figure 8 Pressure contour for converging slope in X-Y at different times: (a) 10 s; (b) 20 s; (c) 30 s 22

Figure 9 Pressure contour for stairs slope in X-Y plane at different times: (a) 10 s; (b) 20 s; (c) 30 s 23

Figure 10 Velocity vectors for plain slope in X-Y plane at different times:(a)10 s; (b) 20 s; (c) 30 s 24

Figure 11 Velocity vectors for converging slope in X-Y plane at different times: (a) 10 s; (b) 20 s; (c) 30 s 25

Figure 12 Velocity vectors for stairs slope in X-Y plane at different times: (a) 10 s; (b) 20 s; (c) 30 s… 26

Figure 13 Pressure contour for plain slope in Y-Z plane reservoir section at different times: (a) 10 s; (b) 20 s; (c) 30 s 27

Figure 14 Pressure contour for converging slope in Y-Z plane reservoir section at different times: (a) 10 s; (b) 20 s; (c) 30 s 28

Figure 15 Pressure contour for stairs slope in Y-Z plane reservoir section at different times: (a) 10 s; (b) 20 s; (c) 30 s 30

Figure 16 Flow rate (frequency-2 Hz and water level-12 cm) for three different shapes (a) plain slope (b) converging slope, (c) stairs slope 34

Figure 17 Flow rate(frequency-2 Hz and water level- 12.25 cm) for three different shapes (a) plain slope (b) converging slope, (c) stairs slope 36

Figure 18 Flow rate (frequency-2 Hz and water level- 12.50 cm) for three different shapes (a) plain slope (b) converging slope, (c) stairs slope… 37

Figure 19 Flow rate (frequency-1.875 Hz and water level- 12 cm) for three different shapes (a) plain slope (b) converging slope, (c) stairs slope 38

Figure 20 Flow rate (frequency-1.875 Hz and water level- 12.25 cm) for three different shapes (a) plain slope (b) converging slope, (c) stairs slope 39

Figure 21 Flow rate (frequency-1.875 Hz and water level- 12.50 cm) for three different shapes (a) plain slope (b) converging slope, (c) stairs slope 40

Figure 22 Flow rate (frequency-1.75 Hz and water level- 12 cm) for three different shapes (a) plain slope (b) converging slope, (c) stairs slope 41

Figure 23 Flow rate (frequency-1.75 Hz and water level- 12.25 cm) for three different shapes (a) plain slope (b) converging slope, (c) stairs slope… 42

Figure 24 Flow rate (frequency-1.75 Hz and water level- 12.50 cm) for three different shapes (a) plain slope (b) converging slope, (c) stairs slope… 43

Figure 25 Comparison of three different shapes between experimental and numerical results for total flow rates versus frequency 44

Figure 26 Comparison of three different shapes between experimental and numerical results for total flow rates versus water level 45

LIST OF TABLES:

Table 1 Regional theoretical potential of wave energy.....1

Table 2 Different Mesh Generation 17

CONTENTS:

Chapter 1 *1-6*

INTRODUCTION

Chapter 2 *7-11*

EXPERIMENTAL APPROACH

Chapter 3 *12-18*

NUMERICAL MODEL

Chapter 4 *19-21*

GRID INDEPENDENCY

Chapter 5 *22-47*

RESULTS AND DISCUSSIONS

Chapter 6 *48-49*

CONCLUSIONS

CHAPTER 1:

1. Introduction

The rise in global energy demand has increased pressure on use of fossil fuel (Non-renewable energy) which has led to serious environmental pollution, threat of global warming and climate change resulting from emission of Green House Gases. Fossil fuels are rather inconsistent and non-reliable while renewal energy sources such as solar, wind and wave energy can supplement the need for energy demand as a clean energy source. Solar and wind power energy are sustainable energy sources that will not run short of, will not pollute the air, and do not have any hazardous effect on the environment. Yet, a downfall persists: they are not readily available. Sun shines for a period of time and must be captured within that time. Moreover, capturing solar energy is difficult. Winds are inconsistent; hence storing solar and wind energy for later use can prove to be a major challenge. An indirect form of solar and wind energy- ocean wave energy, has not been exploited much, and hence has caught the attention of many researchers. The ocean wave energy is the most promising source of energy and made significant advancement in the recent years as many prototypes are currently being tested in different areas of the world[1]. Incorporating with the existing demand, further technological development is essential to prove reliability and robustness of this energy[2]. It has a huge theoretical potential energy that is shown in table 1. However, ocean wave and tidal current are expected to be the most advanced and leading power generation in the future energy supply[3].

Table 1. Regional theoretical potential of wave energy[4].

Region	**Wave Energy** **TWh/yr(EJ/yr)**
Asia	6,200(22.3)
Australia, New Zealand and Pacific Islands	5,600(20.2)
South America	4,600(16.6)
North America and Greenland	4,000(14.4)
Africa	3,500(12.6)
Western and Northern Europe	2,800(10.1)
Central America	1,500(5.4)
Mediterranean Sea and Atlantic Archipelagos (Azores, Cape Verde, Canaries)	1,300(4.7)

In order to utilize the energy reserves of the ocean, much research has been attempted on overtopping wave energy converters (OWEC), which convert the erratic, unstable wave energy to stable potential energy [5]. WECs are still in their primitive stage and a lot of innovative devices have been patented worldwide, but at the expense of low reliability and high manufacturing, construction, installation and maintenance costs among numerous other difficulties. For the purpose of economic research and development of wave energy converters, NWTs have proved to be an extremely effective numeric tool.

Waves are characteristically irregular, and when they are employed in experiments to record overtopping discharges, it is difficult to evaluate and optimize time averaged behaviours. Whereas numerical wave tanks deal with regular waves. To bridge the gap, laboratory experiments have been conducted with several different types of overtopping structures. Three different types of overtopping structures have been designed, first using a CAD software then in the laboratory using plexiglass. Plain slope, Stairs slope and Converging slope-type overtopping structures have been designed along with a reservoir to hold the accumulated discharges.

Physical wave tanks can be of different sizes as per their need; small wave tanks are sufficient for educational purposes but for more advanced requirements such as model testing, large wave tanks are needed to be built. Building the wave tank and acquiring the perfect model has proved to be strenuous. Moreover, testing and re-testing proved to be time consuming and costly. Laborious as it might sound, wave tanks or wave flumes have helped build overtopping structures which convert wave energy to stable energy, helped constructing wave energy converters and even helped establish setup codes. The features of a wave tank include a long, narrow, rectangular enclosure with a wave maker in the end [6]. Wave makers can be of various types, Anbarsooz et al. studied, simulated, and compared piston and flat type of wave maker [7]. Plunger type wave makers are another type of wave makers which are theoretically more complex because the submerged part of the plunger volume changes continuously which causes nonlinear effects. Consequently, fewer studies regarding this type of wave maker are available in literature compared to other wave makers [8]. For our study, wedge type wave makers have been used. Overtopping structures are added in the other end, attached to a reservoir to hold the overtopped discharges. Wave tanks are built by taking

under consideration the type of wave-maker that is most feasible for our study and other parameters and then simulations were carried out which has been compared against experimental results.

1.1. Literature review

Prasad et al. used Commercial Computational Fluid Dynamics (CFD) code ANSYS to design a 3D numerical wave tank (NWT) and generated waves in it. The accuracy and robustness of the numerical code has been validated against experimental data, also at a site in Fiji an actual NWT was constructed. CFD and analytical results compared against each other revealed a difference of 3% further verifying the accuracy of the code [6].

Marques Machado et al. tested two methods of generating waves. Inlet velocity method, where the parameters of the wave is specified by stokes second order equations, and wave-maker method, where piston-type wave maker has been implemented, have been studied. The studies have drawn the conclusion that piston-type wave makers provide better results [9].

Numerical wave tanks can mimic the working of a physical wave tank and can also extend beyond its limitation since they do not face the restraints of laboratory facilities. NWTs allow more extensive insights of the physical tests carried within the limited resources and data. Hence My Ha Dao et al. designed a numerical wave tank with flap paddles and porous beach in the open-source software Open Field Operation and Manipulation (OpenFOAM) similar to the physical wave tank. Laboratory experiments of regular and focused waves were also conducted for validation [10].

Various kinds of overtopping structures have been integrated with WECs. The effect of the design of the device on the time averaged discharges have been investigated. Han et al. carried experiments on multi-level reservoirs. Consequently, the effects of the opening width of the lower reservoir, sloping angles of two reservoirs and the gap height between the reservoirs on overtopping have been studied and investigated against numerical data [5].

Waves are generated in the wave flume with the help of a paddle also known as wave makers. Piston, flap, and wedge type wave makers are a few common examples. These wave makers differ in their motion. Piston type wave makers, generating oscillatory motion, are mostly used in experiments. It has been modelled by Prasad et al. who drew special attention towards the effect of front guide nozzle shape on the flow in the augmentation channel, waterpower and the first stage energy conversion [6]. Dao et al. presented numerical wave tanks with flap paddles and porous beaches by employing regular and focused waves [10].

Over the years, lots of different techniques, methods and models have been used to make the most of the vast energy resource that ocean energy is. S. Shao et al. used a gridless lagrangian approach, incompressible Smoothed Particle Hydrodynamics (SPH) model, for modelling wave overtopping. It was shown that an incompressible SPH model used for overtopping a sloping seawall provides a good overtopping rate [11].

Wave energy converters are a massive success in the present days. Vicinanza, et al. presented their findings on a paper of a hybrid WEC named OBREC[12]. By compounding traditional rubble mound breakwater and front reservoir, the study

showed how electricity can be produced from incoming waves [13]. While Vicinanza focused on that, Musa et al. conducted a research on using the numerical method to demonstrate OBREC [14], [15]. The modelling accuracy was then validated using previous experiments and prediction formula available in the literature.

CHAPTER 2:

2. Experimental approach

2.1. Experimental set-up

The experiment has been conducted in the laboratory of the Islamic University of Technology. The wave tank is a long, narrow rectangular spacing with the upper part open to the atmosphere. It is 211.5 cm long, 28.7 cm wide and 28 cm high and made of smooth glass. At one side of the wave tank, a wedge type wave maker has been linked to the mechanism to allow oscillatory motion in the vertical direction, to initiate wave generation. At the other end lies a reservoir fixed to the wall of the tank to reserve the incident wave water; the reservoir volume is large enough to hold the discharges. Connected to it is the overtopping structures; a discrete plain slope, converging slopes and stairs slope are attached in turn to carry out experiments. The height of the slopes is 14 cm and occupies the entire width of the tank. The sloping wall of the plain slope and converging slope has an angle of 30 the optimum angle shown by Zhen Liu et al.[16]. Converging slope differs from plain slope in that it has structures that reduce the opening width, through which water overtops in a converging manner. As implied by the name, the stair slope has stair-like structure instead of a plain slope. The experimental model of the entire setup is shown in Fig. 1. The edges of the tank, reservoir and overtopping structures have been sealed shut to prevent any kind of water leakage that might hinder experimental accuracies. The water filled wave tank produced regular waves by virtue of the motion employed by the wave maker. The experiment has been conducted for different heights of water to show its effects on overtopping patterns. The wave maker has been connected to an electric motor that enables the

waves to be generated; approximately three to four waves are generated each time the wedge strikes the water body. A switch connected to the electric motor allows the rotational speed to be varied, which in turn changes the frequency. Furthermore, the overtopping pattern has been observed for the different frequencies and the different water levels.

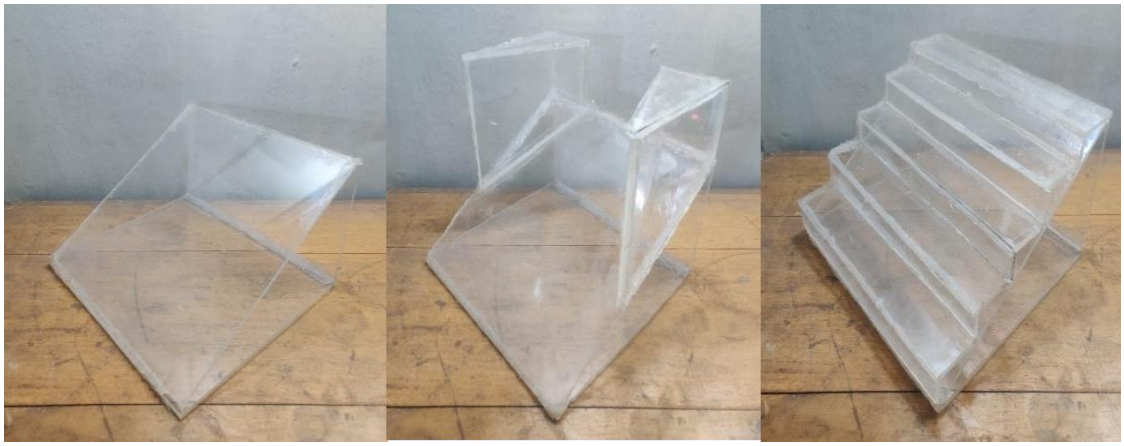

(i) Plain slope (ii) Converging slope (iii) Stairs slope

(a) Physical Model Components

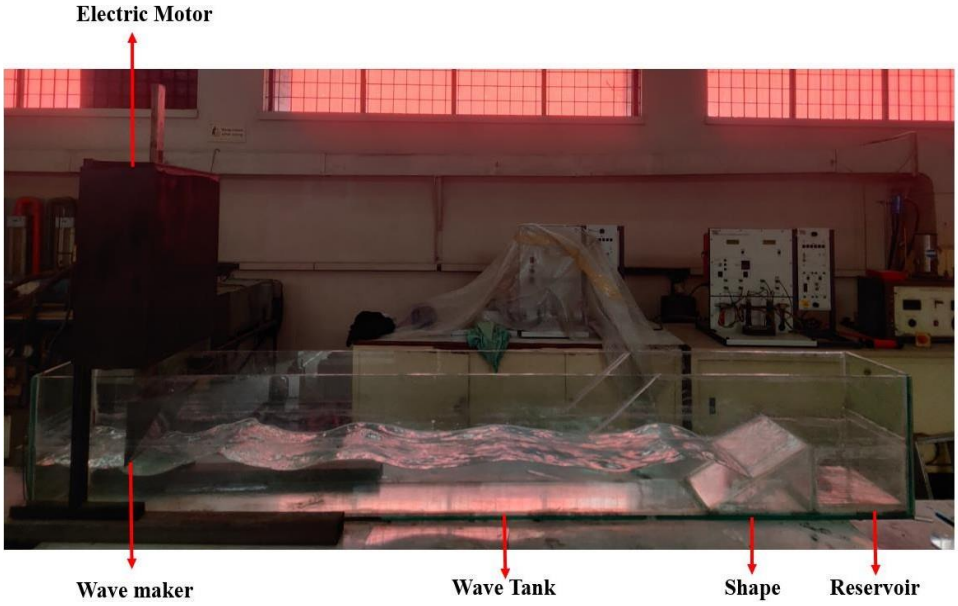

(b) Experimental Wave tank

Fig. 1. Snapshot of the experimental Model

2.2. Experimental procedures

Due to its oscillating motion, as the wave maker hits the water body, regular waves are generated in the wave tank. For every strike of the wave maker, three to four wave cycles are produced. These waves resemble the natural waves produced in oceans due to wind energy. The experiments have been conducted by varying two factors- wave frequency and water height. Experimental data has been collected by varying these factors, and three sets of data have been collected for each of these factors. The same procedure has been repeated for three overtopping structures, showing a comparison of how different shapes affect the flow rate. To begin with, the wave maker has been employed to give rise to waves. The incident regular waves emerge the overtopping structures and strike it with a force that is shown in Fig. 2. The stored potential energy of the waves gets transformed to kinetic energy. The water splashes against the

overtopping structures and tries to overtop it. Waves are produced continuously, splashing against the slope repeatedly, hence accumulating more discharges in the reservoir. A timer and the wave maker is switched on simultaneously. The time-averaged overtopping flow rate has been determined from the volume of the reservoir filled with water and the time measured. To avoid inaccuracy and uncertainties, each experiment has been repeated several times and the results averaged.

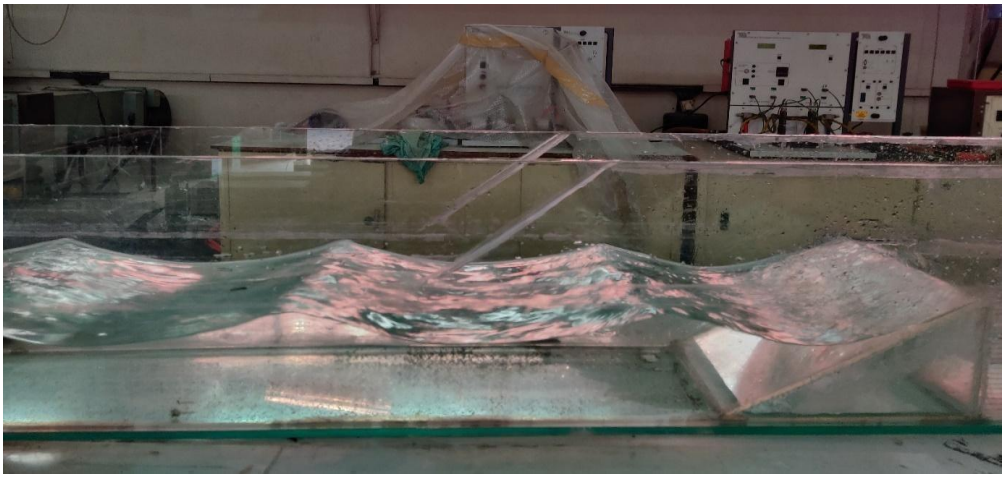

(a)

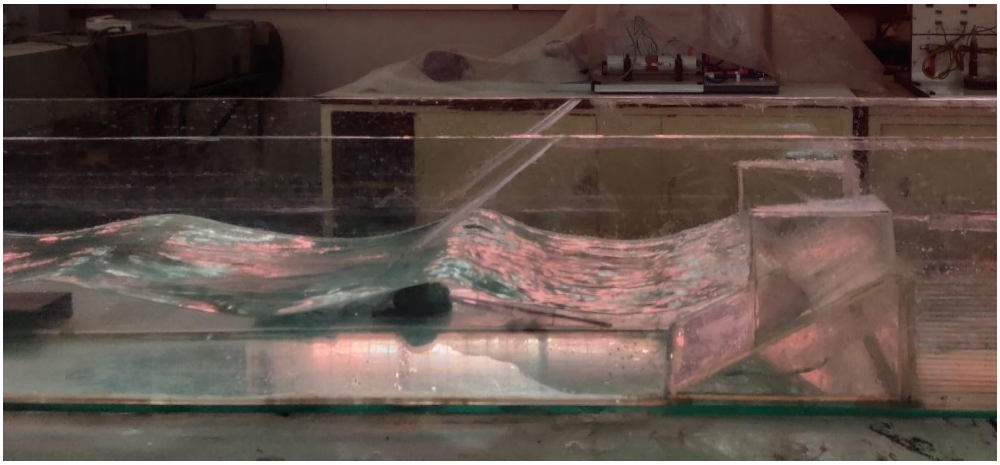

(b)

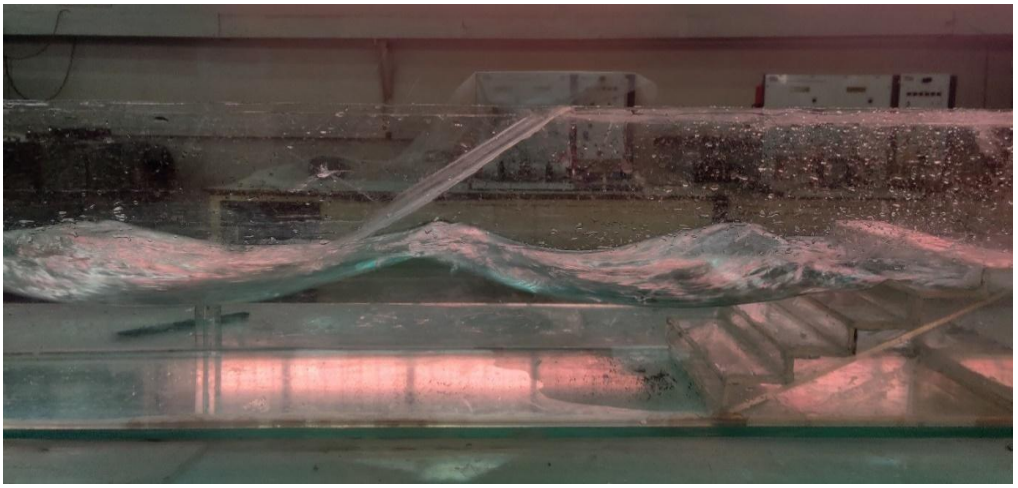

(a)

Fig. 2. Side view of wave tank with the three shapes: (a) plain slope; (b) converging slope; (c) stairs slope

CHAPTER 3:

3. Numerical model

CFD software are Multiphysics software of great accuracy which are highly efficient, detailed solution for free-surface flow problems with human-centric support. Volume of fluid (VOF) method has been incorporated in these software as presented by C. W. HIRT et al., also one-fluid approach for free surface flows has been employed [17]. It is based on 3D Navier-Stokes (NS) equations and continuity equations to simulate flow processes. In this study, CFD codes has been used to simulate a wave flume for NWTs. It has been employed to assess how the experimental data validate the numerical ones, and the pattern and comparison, hence, noted. For accuracy and steadiness of the incident waves, a wedge type wave maker has been set up in the simulation like that in the experimental set-up. Fig. 3 shows the numerical model of different shapes which are used in this study.

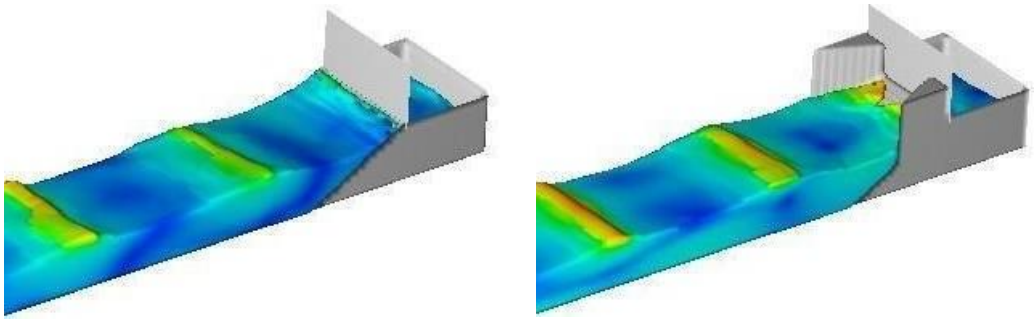

(a) (b)

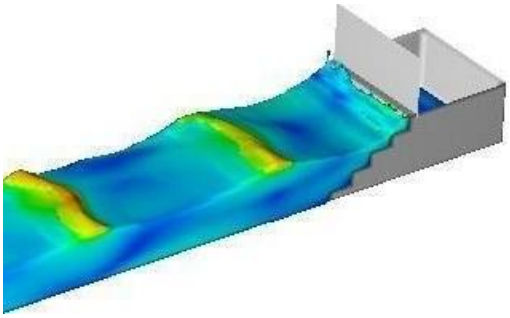

(c)

Fig .3. Wave generation in the NWT for three different shapes: (a) plain slope; (b) converging slope; (c) stairs slope.

3.1. Governing equations

The flow in the wave is solved by using the Reynolds Averaged Navier-Stokes equations coupled with a VOF model. Equations based on the concepts of area fraction (AF) and volume fractions (VF) are used to model the complex geometries of the wave tank. CFD software utilizes a method called the Fractional Area-Volume Obstacle Representation (FAVOR) to formulate the equations for a computational domain. The definition of VF is ratio of open volume to the total volume in a cell, and that of AF is ratio of open area to the total area. For a rectangular structured mesh, there are three AF's namely AFR, AFB, AFT for three cell faces in the direction of increasing cell index. This consequently eliminates the disadvantage in conventional CFD methods for moving objects. The limitation is that moving objects must be at a distance from each other, otherwise causing failure when the mesh distortion is severe. Moreover, re-meshing and automatic meshing is costly, hence not feasible. Hence the general moving object (GMO) model is introduced, allowing a problem to consist of more than one

moving object, and also allows individual moving objects to have independent motion-they can have translational or rotational prescribed motion. For each moving object, a body-fixed reference system and the space reference system is defined. The equations of motion for moving objects are solved by taking account of hydraulic, gravitational and control forces and torques. Furthermore, calculations of the hydraulic force and torque due to pressure and shear stress are done at each time step. With the change in object locations and orientations, area and volume fractions are recalculated each time and for the effect of the moving object displacing fluid, source terms are added in the continuity and the VOF transport equations. The Navier-Stokes equations for momentum and the continuity equation for mass are similar to the partial differential equations (PDE).Hence the 3D wave generation and simulation are differential equations of continuity, mass and momentum conservation laws in the direction of x, y, and z. These equations are based on the law of conservation of mass and momentum and the general continuity equation is:

$$V_f \frac{\partial \rho}{\partial t} + \frac{\partial}{\partial x}(\rho u A_x) + \frac{\partial}{\partial y}(\rho v A_y) + \frac{\partial}{\partial z}(\rho w A_z) = 0 \quad (1)$$

where V_f indicates the fraction of volume to flow and ρ indicates fluid density. Velocity components u, v, and w are in the direction of x, y, and z, respectively. A_x is the fraction of the surface in the direction of x; A_y and A_z are the fraction of the surface y and z axis [18]. The Navier-Stokes equations are:

$$\frac{\partial u}{\partial t} + \frac{1}{V_F}\left(uA_x \frac{\partial u}{\partial x} + vA_y \frac{\partial u}{\partial y} + wA_z \frac{\partial u}{\partial z}\right) = -\frac{1}{\rho}\frac{\partial \rho}{\partial x} + G_x + f_x \quad (2)$$

$$\frac{\partial v}{\partial t} + \frac{1}{V_F}\left(uA_x \frac{\partial v}{\partial x} + vA_y \frac{\partial v}{\partial y} + wA_z \frac{\partial v}{\partial z}\right) = -\frac{1}{\rho}\frac{\partial \rho}{\partial y} + G_y + f_y \quad (3)$$

$$\frac{\partial w}{\partial t} + \frac{1}{V_F}\left(uA_x\frac{\partial w}{\partial x} + vA_y\frac{\partial w}{\partial y} + wA_z\frac{\partial w}{\partial z}\right) = -\frac{1}{\rho}\frac{\partial \rho}{\partial z} + G_z + f_z \quad (4)$$

where (G_x, G_y, G_z) represent mass accelerations and f_x, f_y, and f_z stand for viscosity accelerations.

The motion of a rigid body is generally divided into translational and rotational movements. The velocity of each single moving point is equal to the optional base point velocity plus the velocity that originates from the rotation of the body around the base point. The GMO model considers the mass centre of the body (G) as the base point, for movement in 6 degrees of freedom. The following two equations have been produced from the equations for 6 degree of movement [19]:

$$\vec{F} = m\frac{d\vec{V}_G}{dt} \quad (5)$$

$$\vec{T}_G = [J].\frac{d\vec{\omega}}{dt} + \vec{\omega} \times ([J].\vec{\omega}) \quad (6)$$

The total force and total torque are calculated as the sum of several components as follows:

$$\vec{F} = \vec{F}_g + \vec{F}_h + \vec{F}_c + \vec{F}_{ni} \quad (7)$$

$$\vec{T}_G = \vec{T}_g + \vec{T}_h + \vec{T}_c + \vec{T}_{ni} \quad (8)$$

The continuity and momentum equations for a moving body and the relative transport equations for the volume of the fluid function (VOF) are as follow:

$$\frac{V_f}{\rho}\frac{\partial \rho}{\partial t} + \frac{1}{\rho}\nabla.(\rho\vec{u}A_f) = \frac{\partial V_f}{\partial t} \quad (9)$$

$$\frac{\partial \vec{u}}{\partial t} + \frac{1}{V_f}(\vec{u}A_f.\nabla\vec{u}) = \frac{1}{\rho}[\nabla p + \nabla.(\tau A_f)] + \vec{G} \quad (10)$$

$$\frac{\partial F_f}{\partial t} + \frac{1}{V_f} \sum \vec{u} A \cdot (F_f)_f = -\frac{F_f}{V_f} \frac{\partial V_f}{\partial t} \quad (11)$$

3.2. Turbulence modelling

Much attention must be given to turbulent fluctuation in numerical flow modelling in the study of overtopping waves. Due to limitations such as computer memory and processing time, turbulence cannot be accounted for using equations of mass and momentum conservation. Instead, CFD software has turbulence models. For wave breaking and overtopping models, the flow becomes highly rotational and complex in nature; hence a more advanced description of the flow dynamics is required. Variation in pressure and velocities can be accounted for and resolved using the Direct Numerical Simulation (DNS). Moreover, it can be implemented in multi-phase flows as shown in J. Reveillon et al. [20]. But the computational cost is high thus rendering it unaffordable to be used in engineering studies. Large eddy simulation offers better computational accuracy and efficiency; the basic idea is to directly compute resolvable turbulent flow structures by the computational grid and approximate the features that are too small to be resolved. However, its requirement of a very fine grid which is not easily achievable, makes it still infeasible for engineering applications. On the other hand, Reynolds Averaged Navier-stokes (RANS) model has gained much reputation for being sophisticated and has been widely used in many engineering applications. As the name implies, this model is based on averaging the flow equations. Transport equations are added for more closure of the flow equations and these strongly replicate the behaviour of flow turbulence and closes turbulence stresses. To address the turbulence effects in the simulation, the most popular and extensively used model, which is comprised of

two transport equations for the turbulent kinetic energy k and its dissipation ε, the k-ε model is used.

3.3. Baffles

For measuring the flow rate in the simulation, a baffle, which acts as the flux surface diagnostic tool, has been introduced in the numerical wave tank. The baffle has been placed just after the slopes to capture the discharges flowing to the reservoir. It is thin and porous and has been placed vertically in front of the reservoir to compute the overtopping discharges.

3.4. Boundary conditions

While solving Reynolds Averaged Navier-Stokes and continuity equations, it is a necessity that boundary equations are applied. As shown in Fig. 4, the entire wave tank is a solid region and bounded within it is the fluid; consequently, wall boundary condition has been used around the tank. The front boundary (minimum y) always remains as ‘wall’ boundary condition because it remains as a solid region throughout, and the back boundary (maximum y) continues as ‘symmetry’ boundary condition in which defining any input is not needed but it is essential for the boundary condition to be applied correctly. This kind of boundary conditions are mainly used in viscous flows for modelling slip walls. While processing the CFD simulation, the boundary condition helps decrease the computational effort. Considering the mesh block 2 in the figure, the left boundary (minimum x) and the right boundary (maximum x) are both defined as the volume flow rate boundary condition. The left and right boundaries in the mesh block 3 are specified as volume flow rate and wall boundary conditions, respectively.

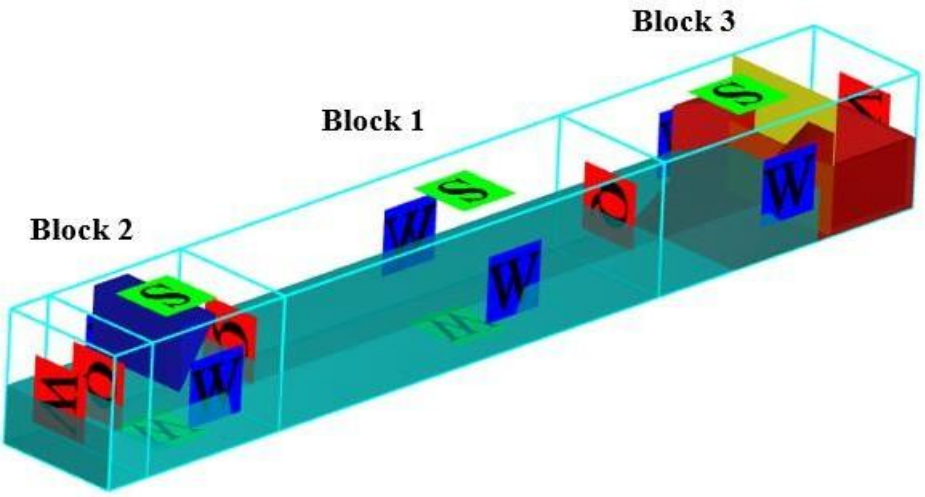

Fig.4. Boundary conditions of the numerical wave tank

CHAPTER 4:

4. Grid Independency

Table 2. Different Mesh Generation

	Cell number (block 2 & 3)
1	300000
2	500000
3	700000

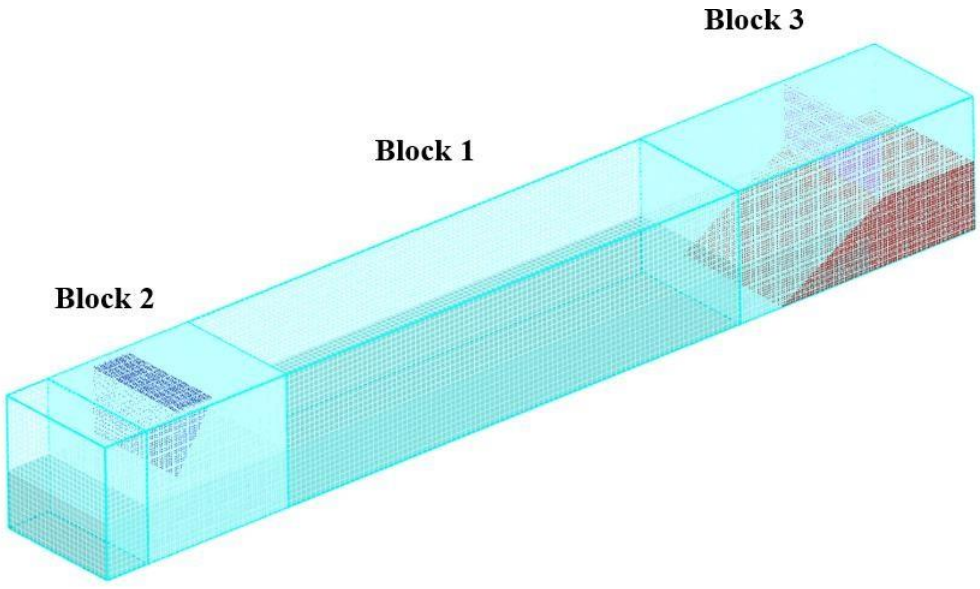

(a)

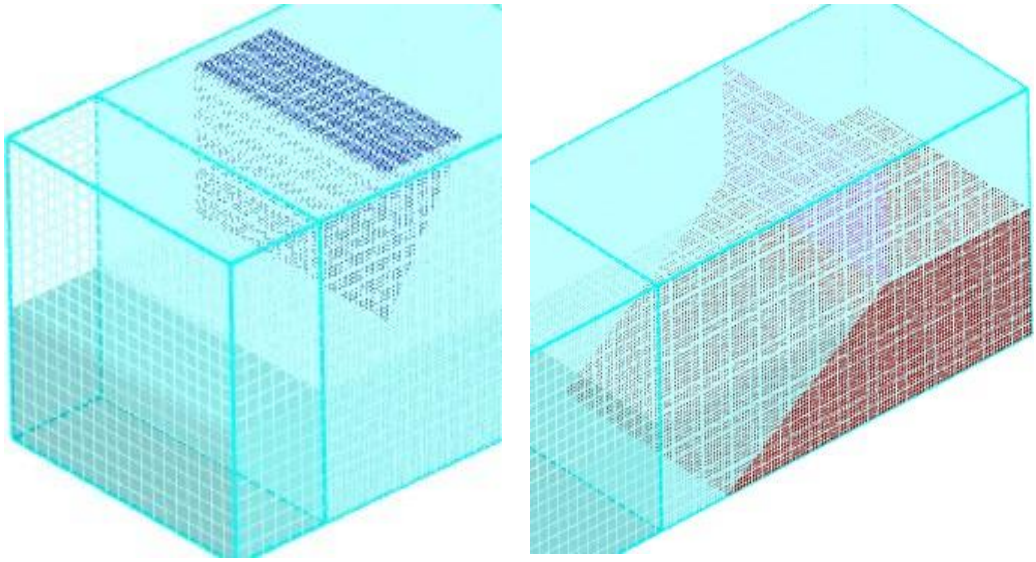

(b) (c)

Fig. 5. Meshing of geometry: (a) The entire wave tank; (b) Wave maker section and (c) Plain slope section

Apart from the structured meshes that are generated for the simulation, two more mesh blocks with different cell size, have been incorporated to demonstrate the flow description with greater accuracy. The structured mesh is relatively easy to generate and requires lesser time, hence for areas of interest nested mesh blocks can be included with smaller grid size [21], [22]. This improves both simulation time and accuracy. Mesh block 1 has larger grids compared to blocks 2 and 3 where the wedge movement and overtopping takes place respectively. The entire domain need not be maintained at smaller grid size, instead the parts where precision is required, smaller grid sizes have been incorporated. The meshing details has been shown in fig. 5. In the figures a, b and c different section of the wave tank with its grid sizes have been depicted. In order to enhance the accuracy of the solution, it is essential to include sufficient mesh grids. Grid study helps to ease simulation time and keep precision [23]. Therefore, three grids

have been generated and the mesh cell sizes employed are 300000, 500000 and 700000 cell numbers, respectively for mesh block 2 and mesh block 3 which has shown in table 2. The results of velocity in the x direction are represented in Fig. 6. The results of velocity for 500000 cells and 700000 cells are close to each other which indicates that grid independency is achieved. Consequently, the grid with 500000 cells is used in this study. Hence, this cell size was chosen for all the simulations of this present research.

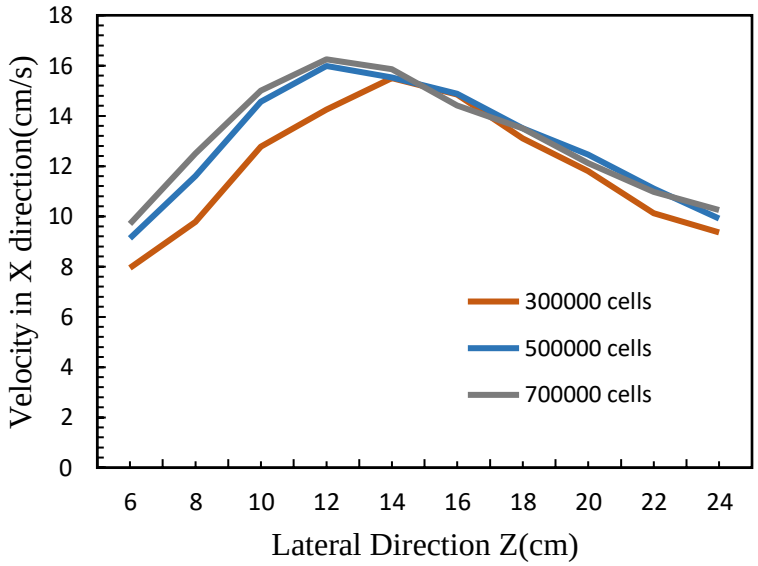

Fig. 6. Comparison of flow rate for different cell numbers

CHAPTER 5:

5. Results and Discussion

5.1 Effect of pressure contour on the overtopping structures

To understand the effect of different shapes on overtopping discharges better, hydrostatic pressure contour has been shown for each set-up as shown in Figs. 7-9. As depicted in the pressure contours, wave generation begins at the start of the tank because of the wedge movement, the waves propagate and strike the overtopping structures. Four wave peaks are seen to be generated and the pressure is highest at the peaks. Velocity vectors seem to point from the wave peaks towards the end of the wave tank as should be which is shown in Figs. 10-12. The focus of this article is to observe the effects of the devices on overtopping; hence, a comparative study can be done from the Figs. 7-9 as well. For constant wave height and frequency, the outcomes are examined for different times and the same time frame is taken for all the shapes. It is visible from Fig. 8 that the converging slope has most water accumulated in the reservoir, meaning it has the highest flow rate. The overtopping discharge in the reservoir helps to predict the better shape to store water in the reservoir that is shown in Figs. 13-15. Also, one unique thing observed is that the flow is not dispersed throughout the structure but is concentrated through a small width, the flow has been converged. The stair slope has the least amount of water accumulated hence least flow rate as noticed in the experiment as well; the results are thus validated.

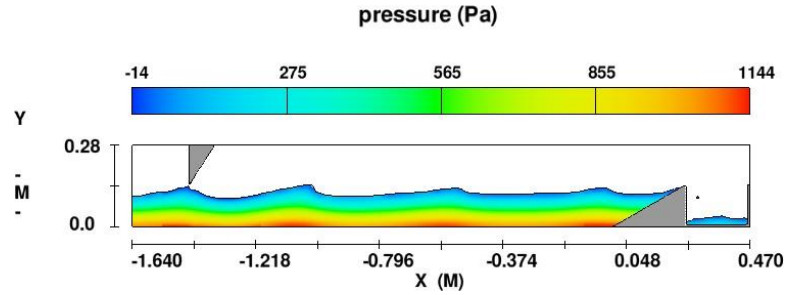

(a)

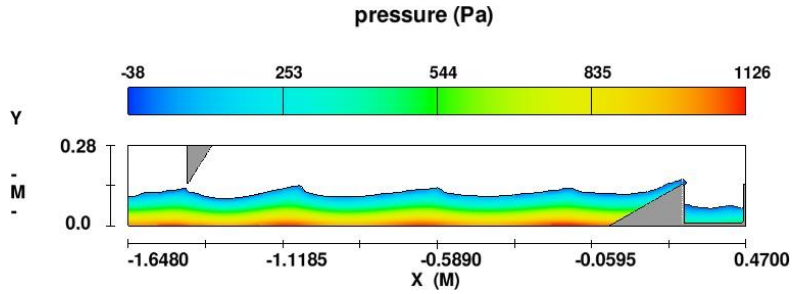

(b)

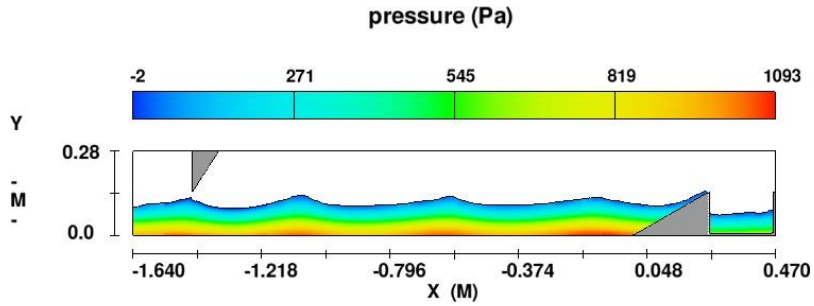

(c)

Fig. 7. Pressure contour for plain slope in X-Y plane at different times:(a) 10 s; (b) 20 s; (c) 30 s

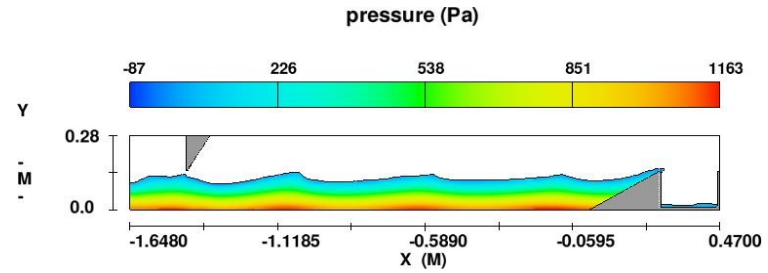

(a)

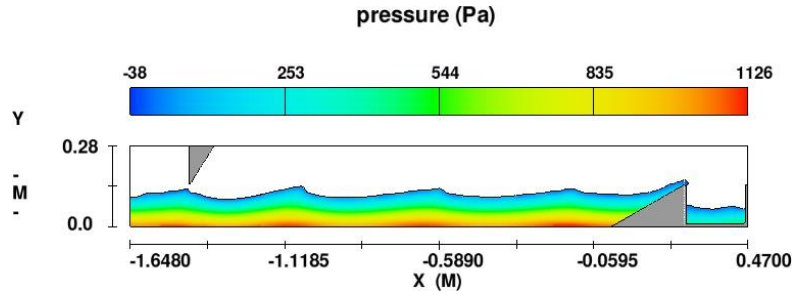

(b)

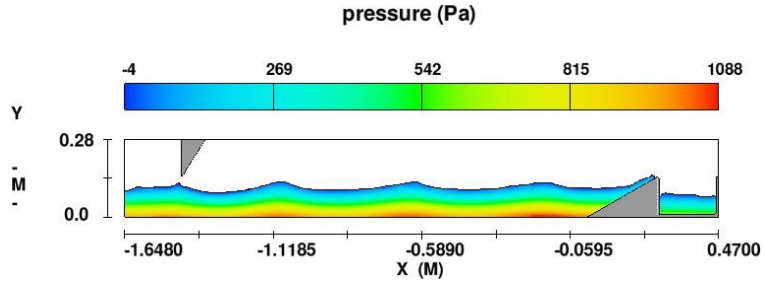

(c)

Fig. 8. Pressure contour for converging slope in X-Y at different times: (a) 10 s; (b) 20 s; (c) 30 s

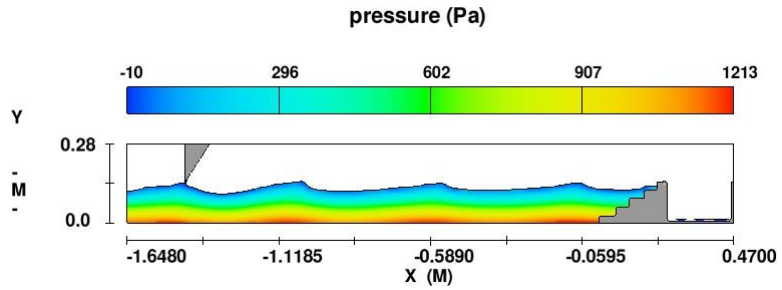

(a)

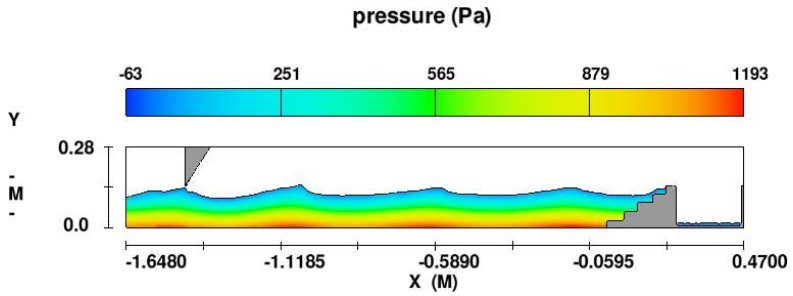

(b)

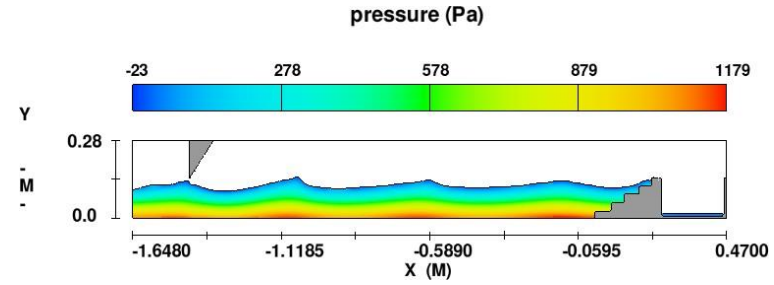

(c)

Fig. 9. Pressure contour for stairs slope in X-Y plane at different times: (a) 10 s; (b) 20 s; (c) 30 s

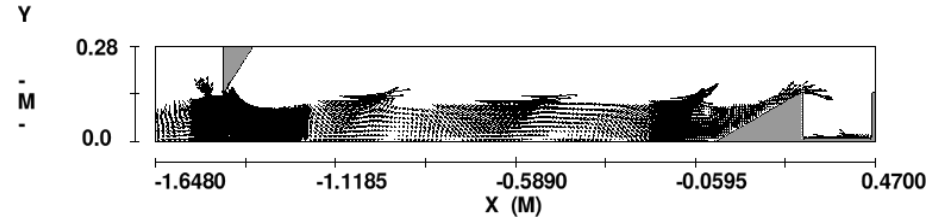

(a)

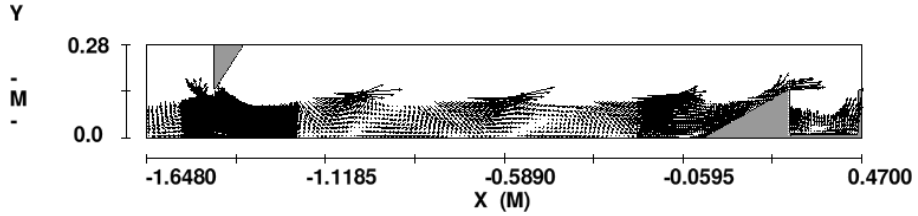

(b)

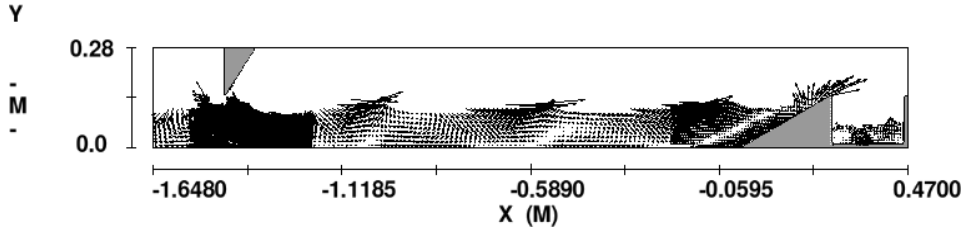

(c)

Fig. 10. Velocity vectors for plain slope in X-Y plane at different times:(a)10 s; (b) 20 s; (c) 30 s

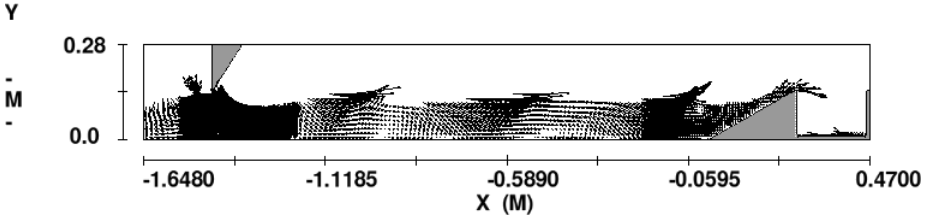

(a)

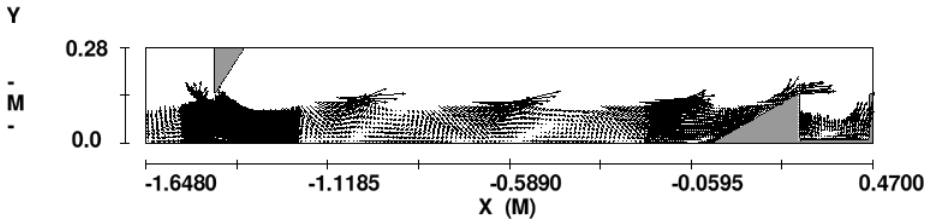

(b)

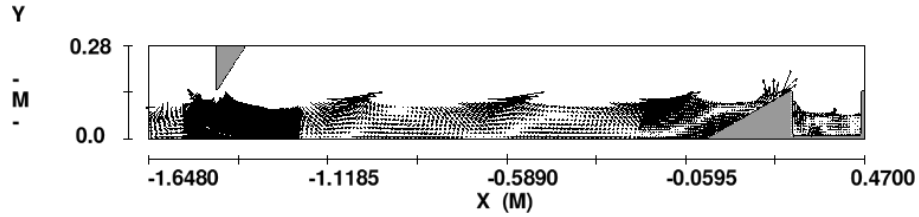

(c)

Fig. 11. Velocity vectors for converging slope in X-Y plane at different times: (a) 10 s; (b) 20 s; (c) 30 s

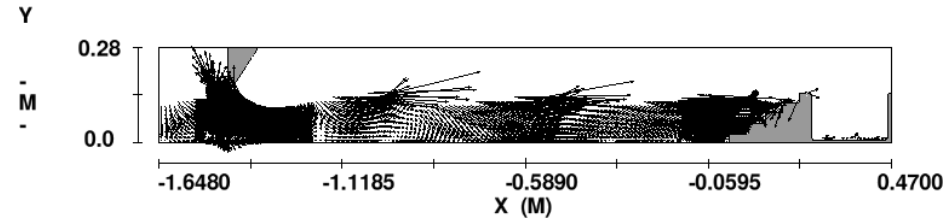

(a)

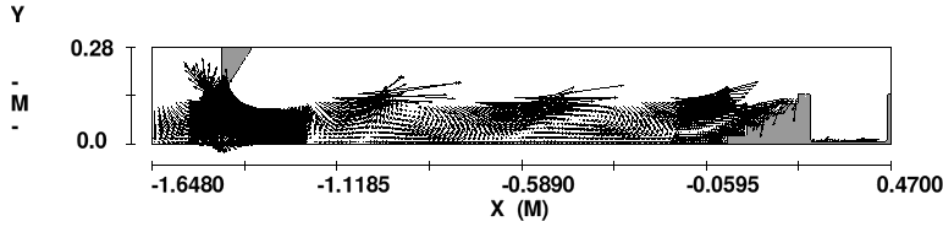

(b)

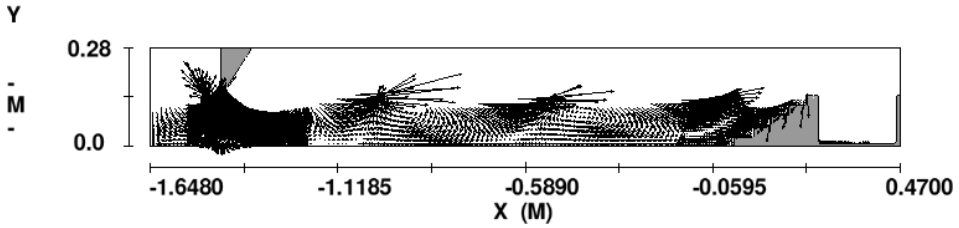

(c)

Fig. 12. Velocity vectors for stairs slope in X-Y plane at different times: (a) 10 s; (b) 20 s; (c) 30 s

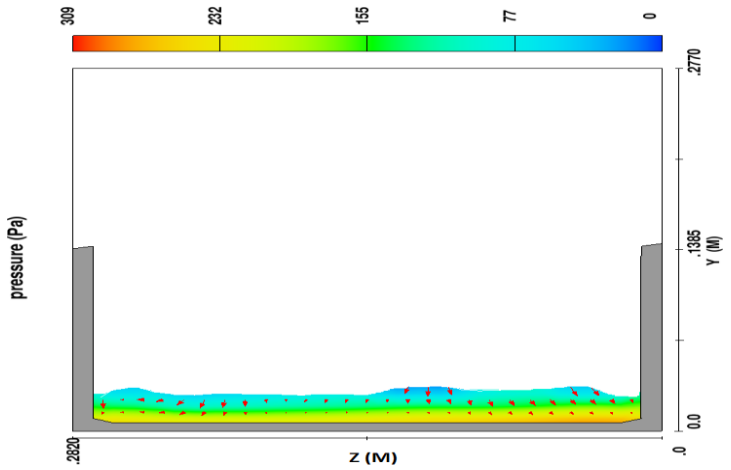
309
232
155
77
0
pressure (Pa)
.2770
.1385
Y (M)
0.0
.0
.2820
Z (M)

(a)

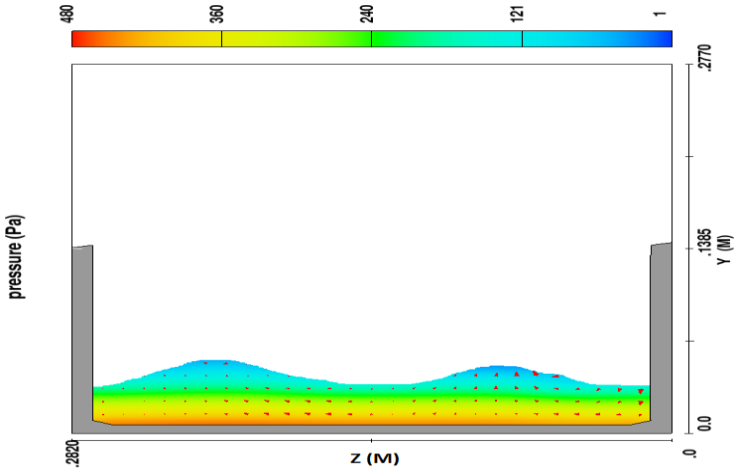
480
360
240
121
1
pressure (Pa)
.2770
.1385
Y (M)
0.0
.0
.2820
Z (M)

(b)

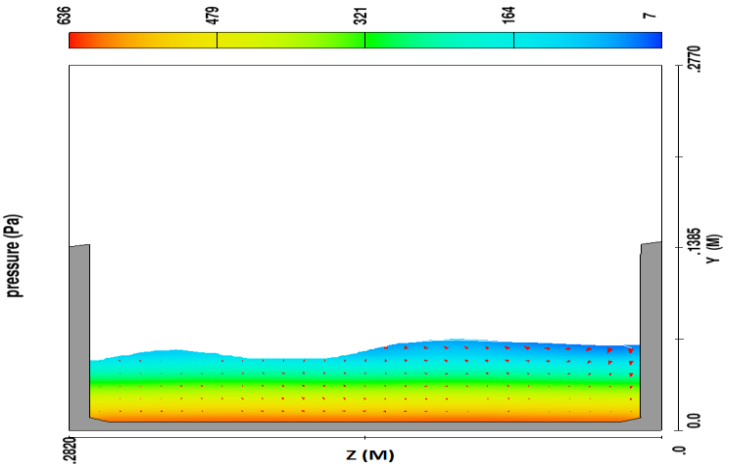
636
479
321
164
7
pressure (Pa)
.2770
.1385
Y (M)
0.0
.0
.2820
Z (M)

(c)

Fig. 13. Pressure contour for plain slope in Y-Z plane reservoir section at different times: (a) 10 s; (b) 20 s; (c) 30 s

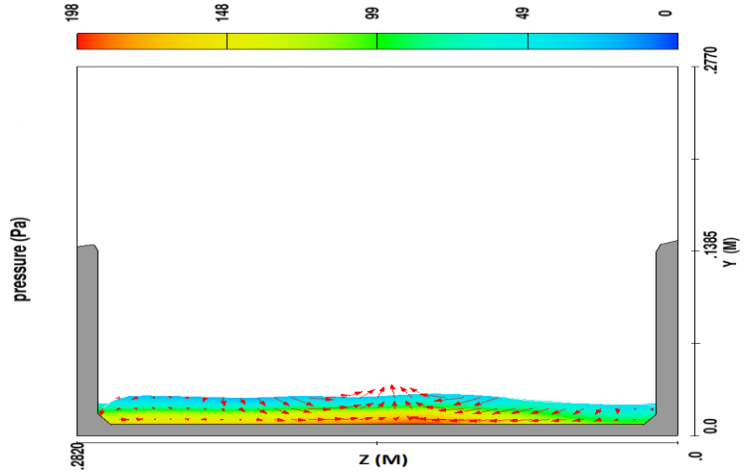

(a)

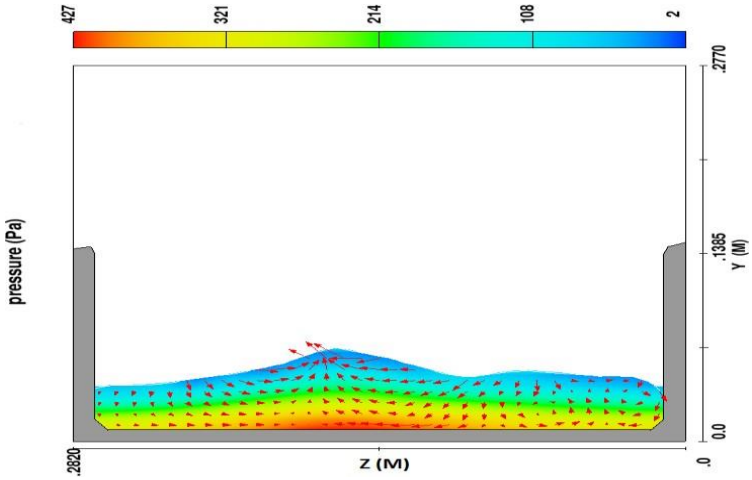

(b)

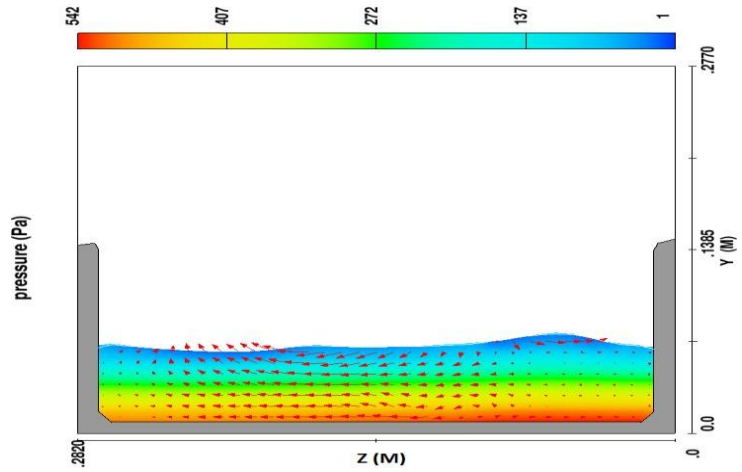

(c)

Fig. 14. Pressure contour for converging slope in Y-Z plane reservoir section at different times: (a) 10 s; (b) 20 s; (c) 30 s

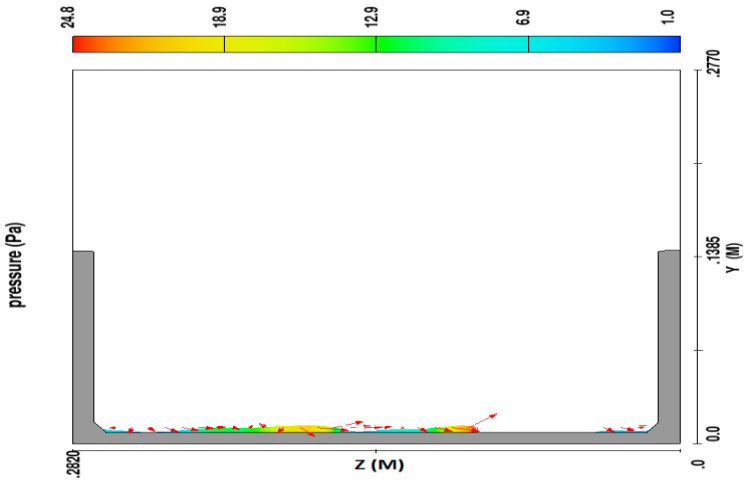

(a)

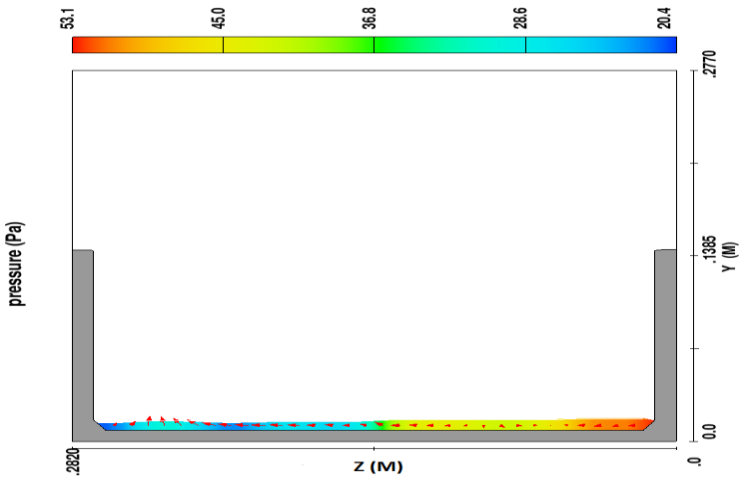

(b)

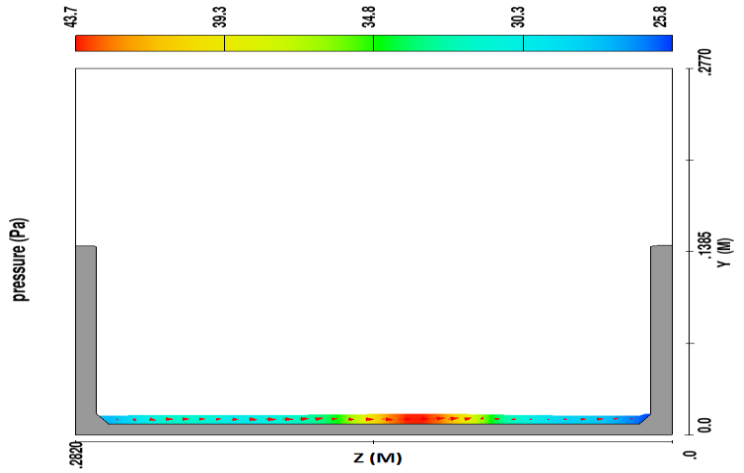

(c)

Fig. 15. Pressure contour for stairs slope in Y-Z plane reservoir section at different times: (a) 10 s; (b) 20 s; (c) 30 s

5.2 Effect of overtopping structures on overtopping discharge

In this study, three different shapes of overtopping structures have been employed to study the overtopping behaviour. The performance of each shape was evaluated for three different water levels including 12 cm, 12.25 cm and 12.5 cm. Since we are

observing the influence of wave height of different overtopping structures, it is imperative that one frequency is taken to be constant for various water heights. Moreover, three different frequencies have been incorporated for detailed studies. All the data obtained have been plotted on graphs to study and compare the effects.

5.2.1 Plain slope

A plain slope has been constructed with a sloping angle of 30 degree. Fig. 16(a)-24(a) shows the numerical and experimental comparison of flow rate when plain slope has been used. As can be observed, with the increase in frequency, the flow rate also increases. Also, maximum overtopping discharges are observed for water height of 12.5 cm.

5.2.2 Converging slope

The second shape is a converging slope; the structure consists of a converging structure on top of a sloping ramp that concentrates the flow of water, which was otherwise dispersed throughout the structure. The wave maker produces waves which strike the slope first, then water climbs up the slope and enters the converging section. As the water enters the converging section, it accumulates the discharges sending it to the reservoir which collects it. From both numerical and experimental results shown in Fig. 16(b)-24(b), it is clear that the overtopping flow rate for converging slope gives better results compared to the plain slope. Maximum flow rate for converging slope has been observed for a frequency of 2 Hz and height of 12.5 cm which is 105.33 cm^3 (experimental) and 112.33 cm^3 (numerical).

5.2.3 Stair slope

Stair slope is another unique and the third shape consisting of five steps that has been employed in the study. It gives the worst result out of all three shapes. Because of its characteristic shape, much water fails to climb upwards. The water waves propagate, strike the steps like structure and are reflected back. Only a small volume of water at high frequency makes it to the reservoir.

The major focal point of the analysis is the overtopping behaviour; experiments have been conducted that depicts the effect perfectly. The study negates wave reflections and wave loadings, and the main concentration has been put on the change in flow rate pattern for each overtopping structure. In this section, a graphical comparison has been made for numerical and experimental solutions for volumetric overtopping discharge against time. For each overtopping structure, frequency of the wave maker and height of the water level is varied and in total 27 tests have been carried out. The numerical results are in good accordance with the experimental one with a little error caused by the limitations while performing the experiment and due to the complications of specifying the actual scenario during numerical simulation configuration. In Fig. 12 for a frequency of 12 Hz and height of 12 cm, three cases have been shown. The first thing to observe is that maximum overtopping occurs for converging slopes with a discharge of almost 90 cm^3. Moreover, a good agreement is observed between the numerical and experimental graph plots. Comparatively for a plain slope, for which a lot of research has been conducted previously by, has lower overtopping discharge[5]. Stair slopes have the lowest accumulated discharge as well as the presence of a significant difference between the numerical and experimental results. The wave tank was not high enough and due to the characteristic shape of the stairs, a good amount of water kept splashing in different directions and failed to accumulate in the reservoir; hence at 60s

only 10 cm^3 flowrate is noted experimentally whereas numerically, it rises to almost 16 cm^3. In Fig. 17, Fig. 20 and Fig. 23, a higher water level of 12.25 cm is taken and its effect thus observed. An increase in overtopping is noticed for all the shapes. But the effect is not significant enough for stair slopes. A little more increase in water level almost doubled the flowrate for stair slope; experimentally the flowrate value is 34.33 cm^3 and numerically 25.67 cm^3 after 60s. Consequently, flowrate increased for the other shapes as well with converging slope having the highest flowrate. More tests have been executed to understand the effect of change in frequency on overtopping behaviour. The frequency has been decreased to 1.875 Hz and the results are plotted. While there is an overall decrease in discharges for every shape, the effect is particularly significant for stair slopes; the flowrate decreases to as much as 2 cm^3. However, the decrease in flowrate is not particularly notable for converging slopes and it continues to maintain a high discharge. The effect of rising the water level is only worth mentioning for stair slopes since the flowrate increases significantly at higher water levels for the same frequency. The frequency is further decreased to 1.75 Hz and the flowrate observed for different water levels. For stair slopes, the rate is low which increases with water height and the converging slope continues to produce high overtopping discharges with a little fluctuation.

The behaviour of overtopping structures for different frequencies has been plotted in a single graph in Fig. 25. As exhibited in the graph, stair slopes have much lower flowrate for every frequency compared to the other shapes, plain slopes have intermediate, whereas converging slopes have the highest flow rate for all frequencies. Fig. 26. shows a similar trend when total flowrate was plotted against water level. The flowrate

increases with water level height; but the effect is more significant for stair slope and plain slopes.

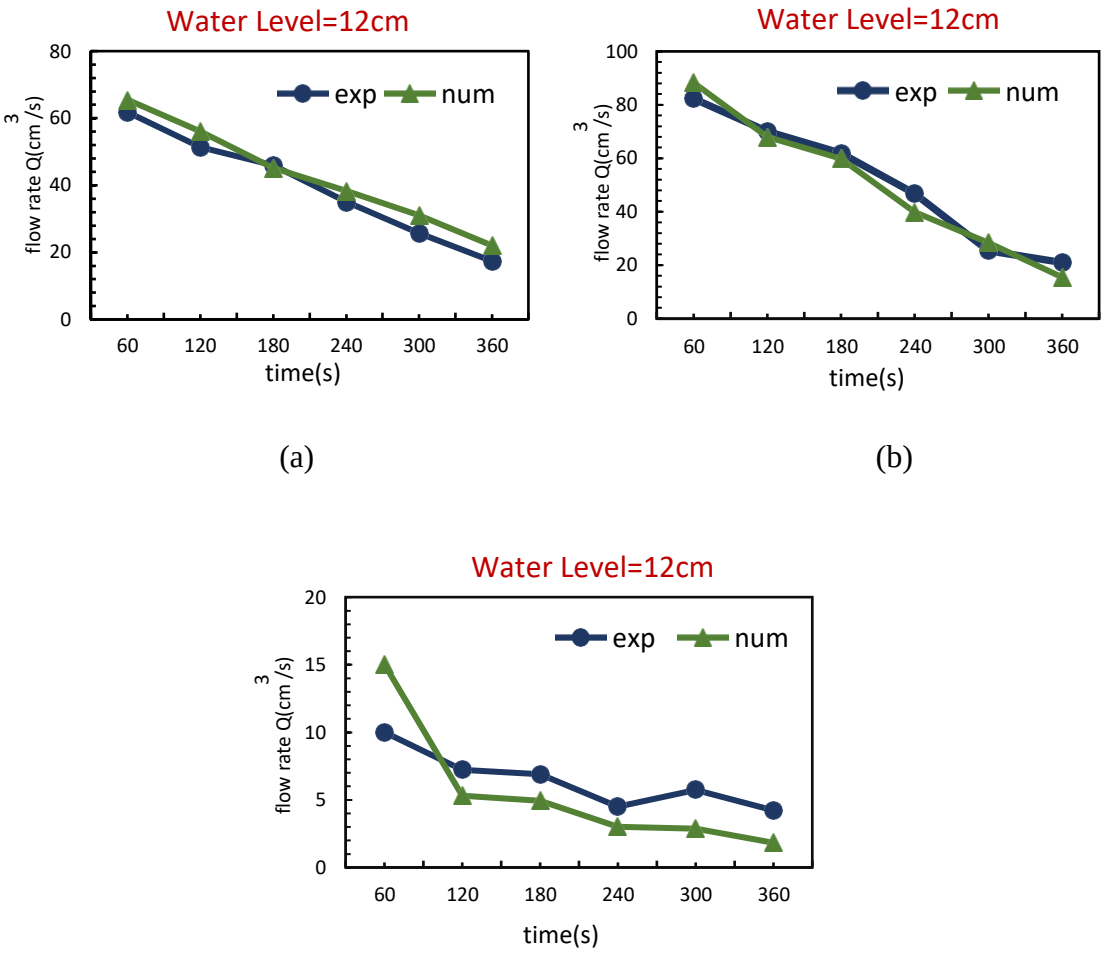

Fig. 16. Flow rate (frequency-2 Hz and water level-12 cm) for three different shapes (a) plain slope (b) converging slope, (c) stairs slope

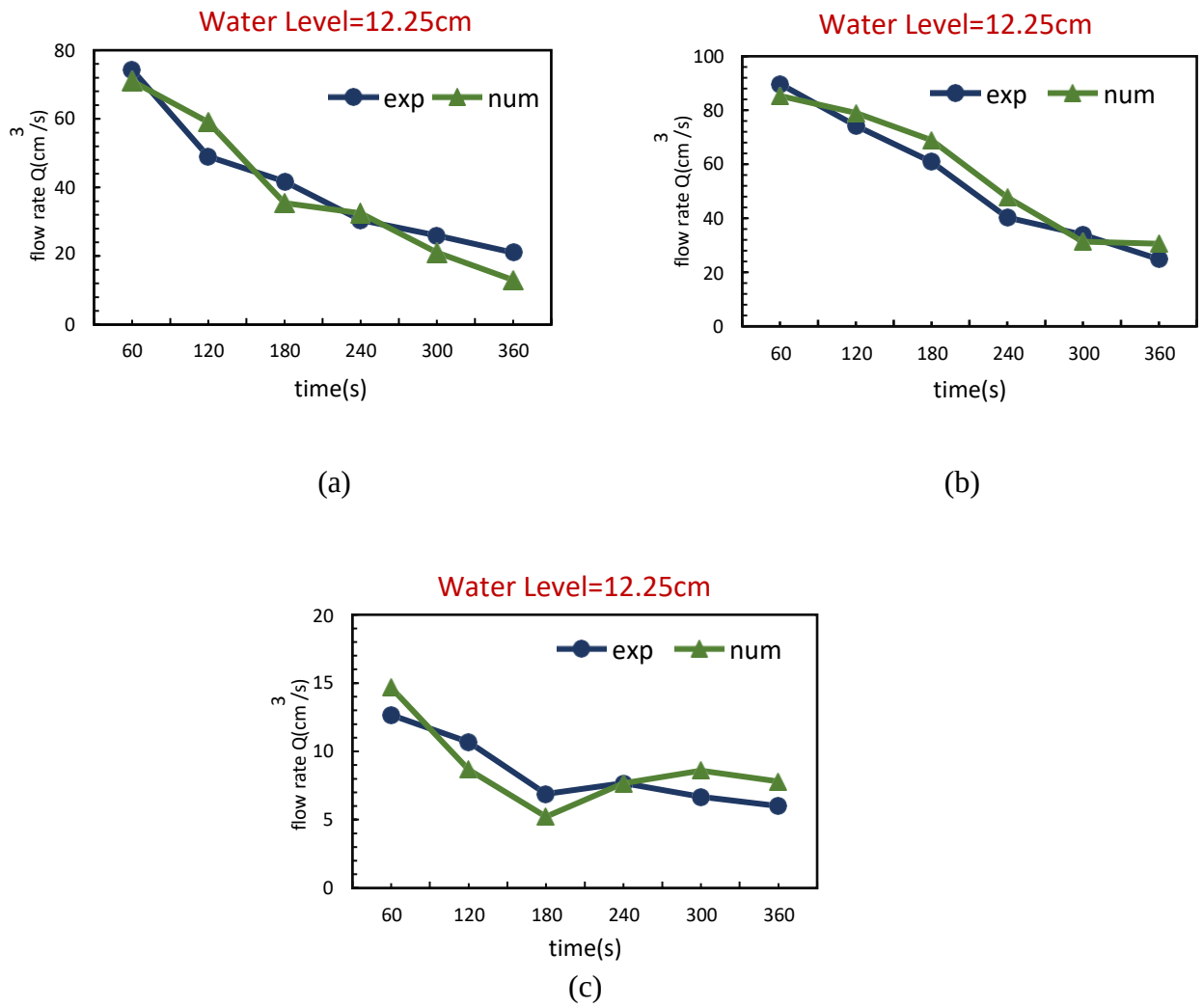

Fig. 17. Flow rate(frequency-2 Hz and water level- 12.25 cm) for three different shapes (a) plain slope (b) converging slope, (c) stairs slope

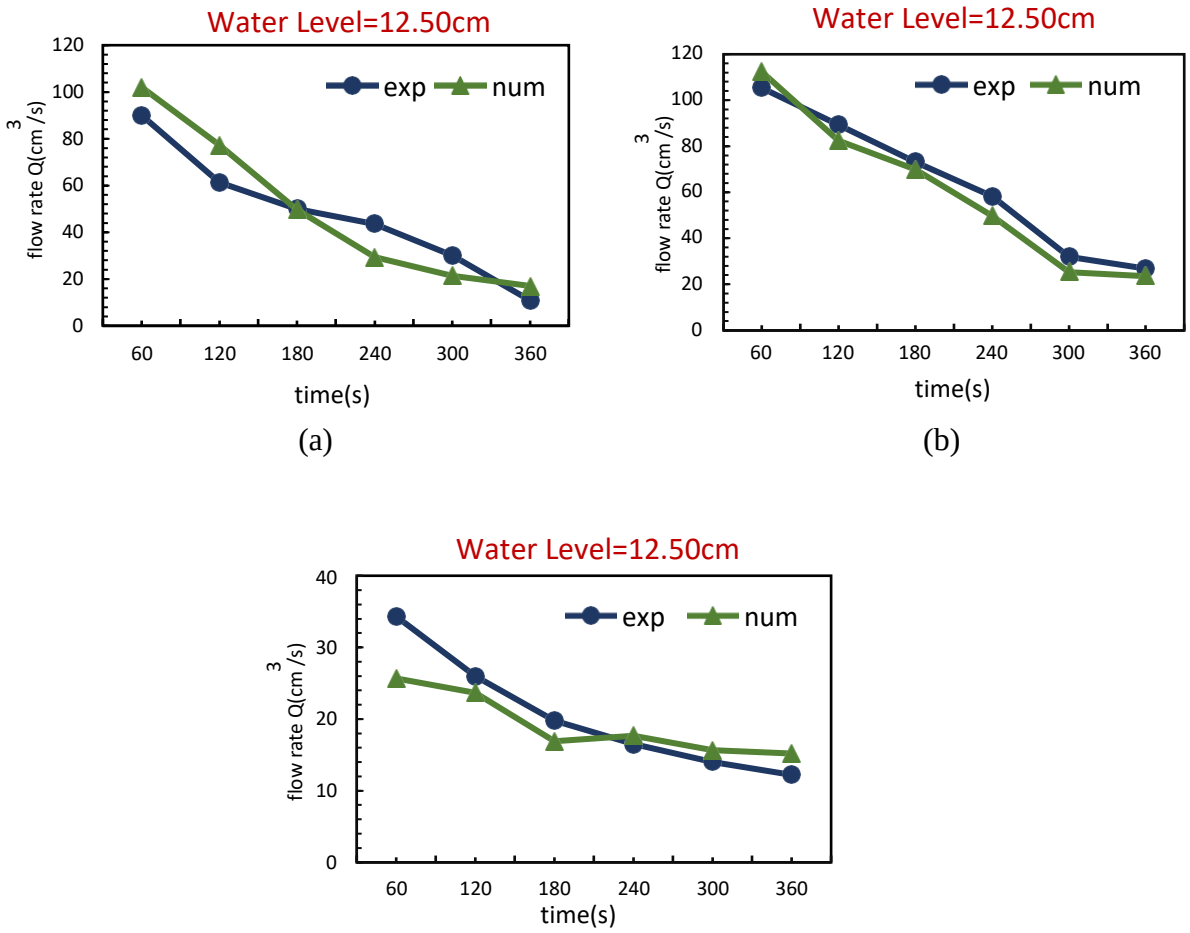

Fig. 18. Flow rate (frequency-2 Hz and water level- 12.50 cm) for three different shapes (a) plain slope (b) converging slope, (c) stairs slope.

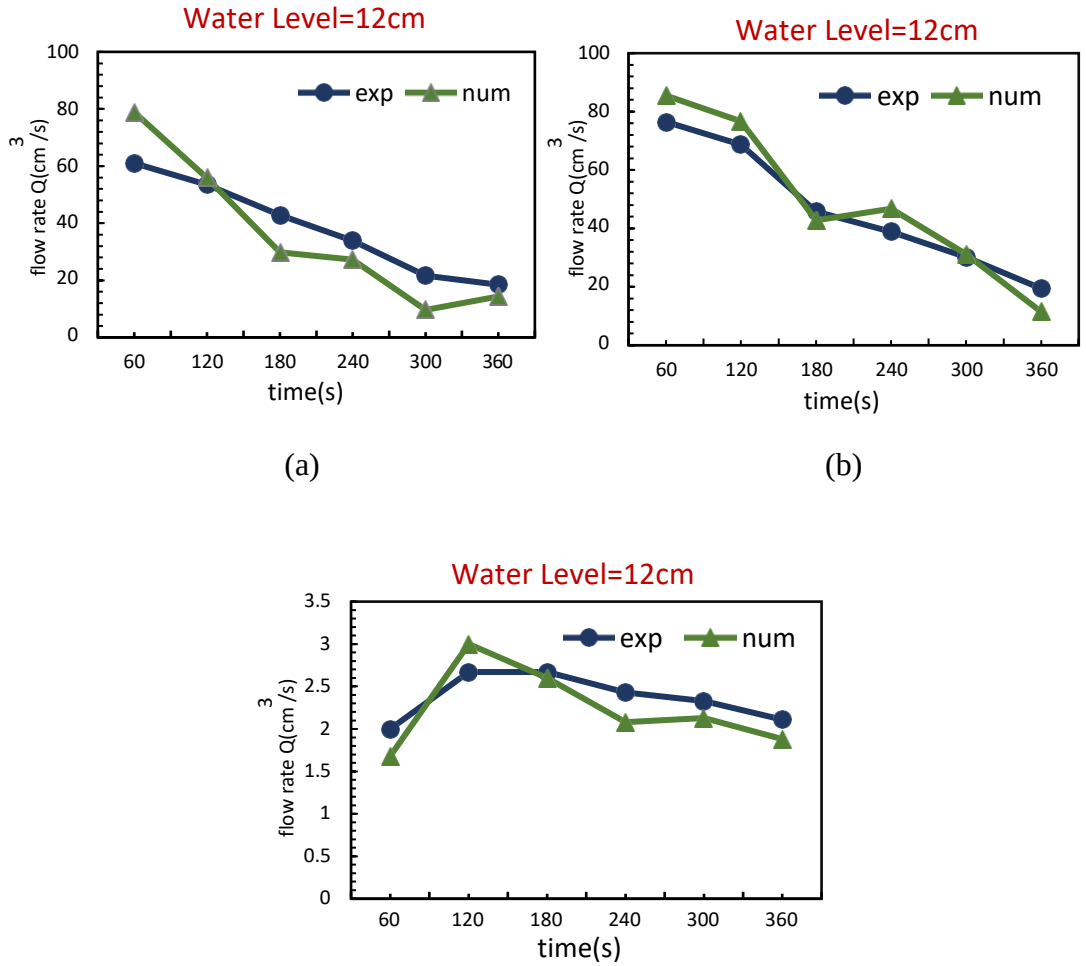

Fig. 19. Flow rate (frequency-1.875 Hz and water level- 12 cm) for three different shapes (a) plain slope (b) converging slope, (c) stairs slope.

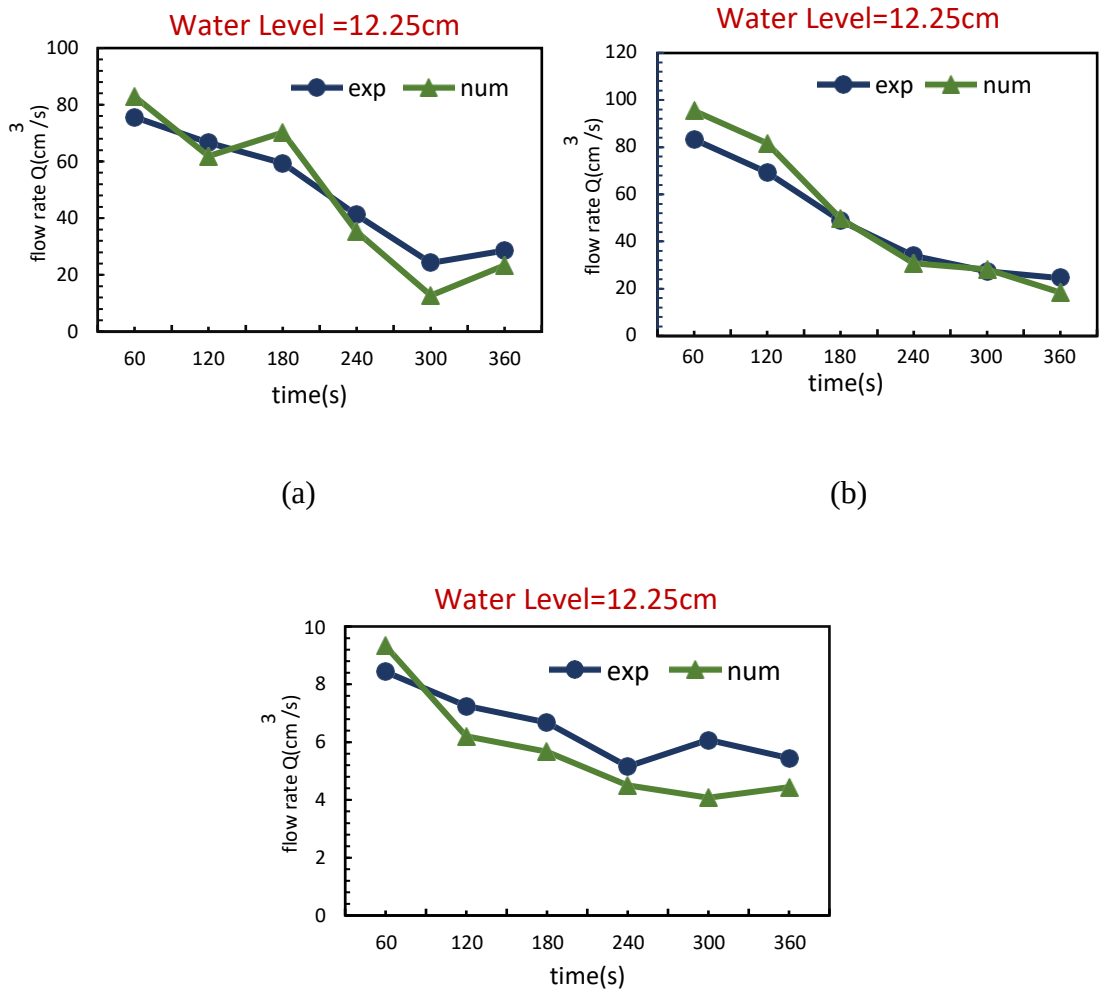

Fig. 20. Flow rate (frequency-1.875 Hz and water level- 12.25 cm) for three different shapes (a) plain slope (b) converging slope, (c) stairs slope.

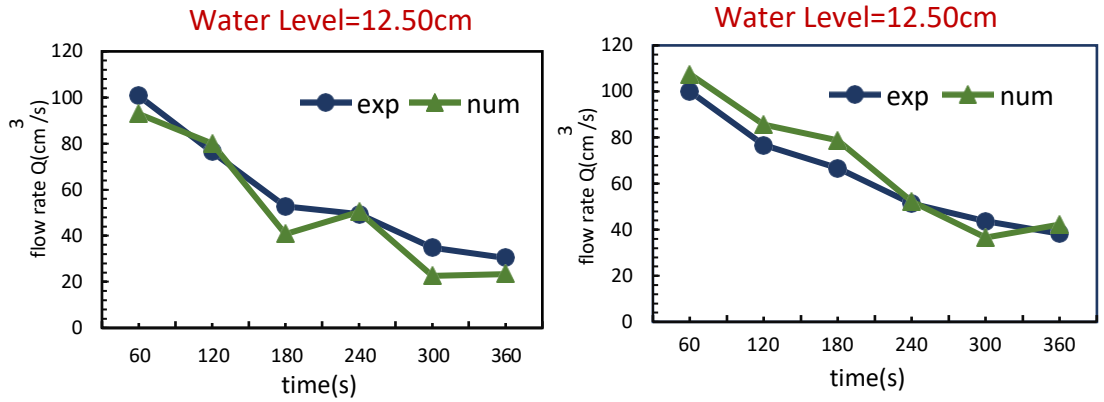

(a)

(b)

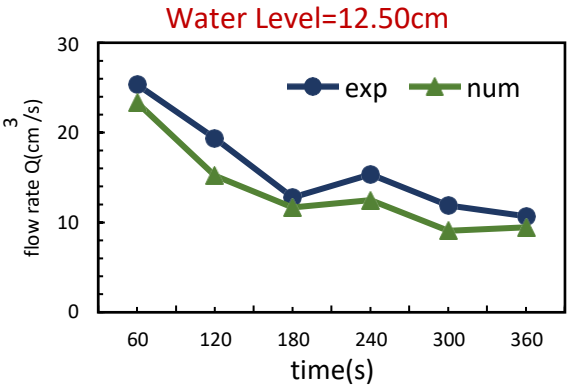

(c)

Fig. 21. Flow rate (frequency-1.875 Hz and water level- 12.50 cm) for three different shapes (a) plain slope (b) converging slope, (c) stairs slope.

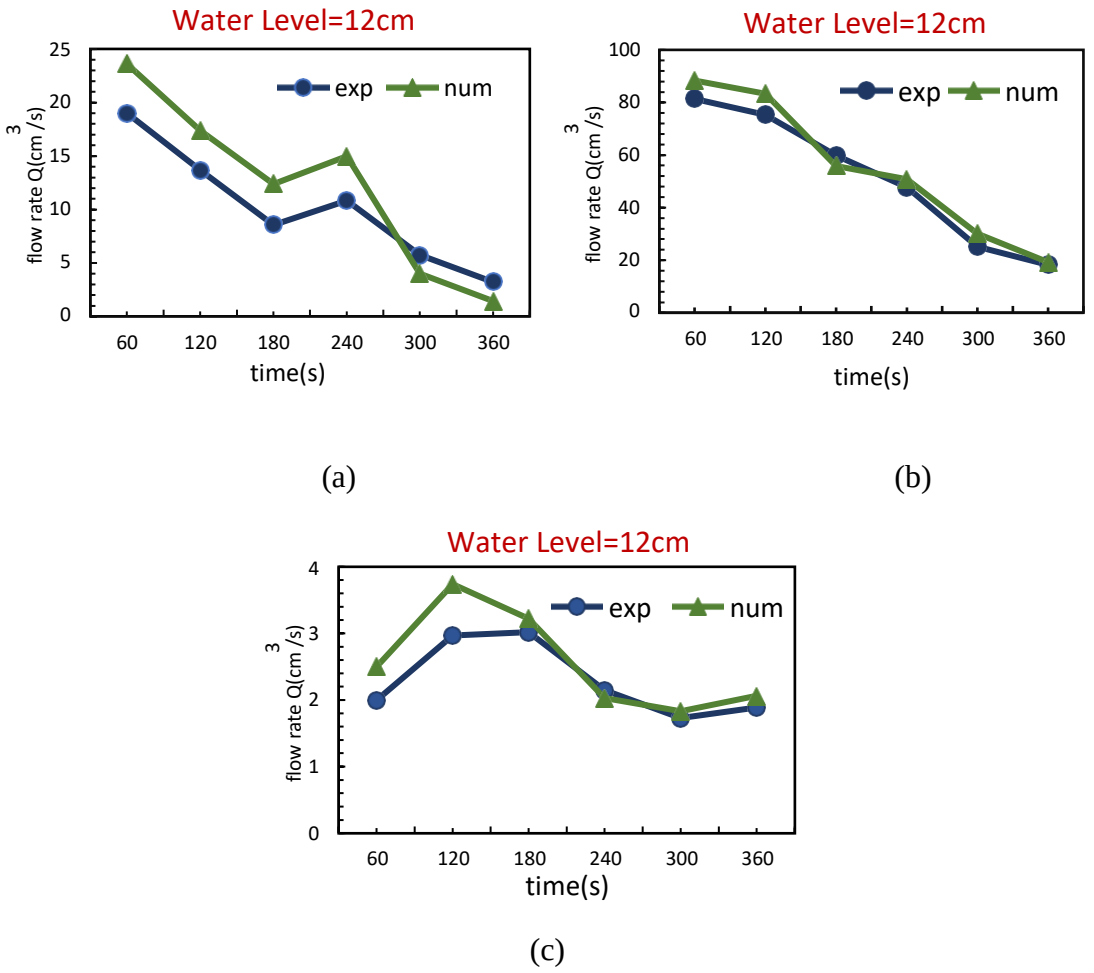

Fig. 22. Flow rate (frequency-1.75 Hz and water level- 12 cm) for three different shapes (a) plain slope (b) converging slope, (c) stairs slope.

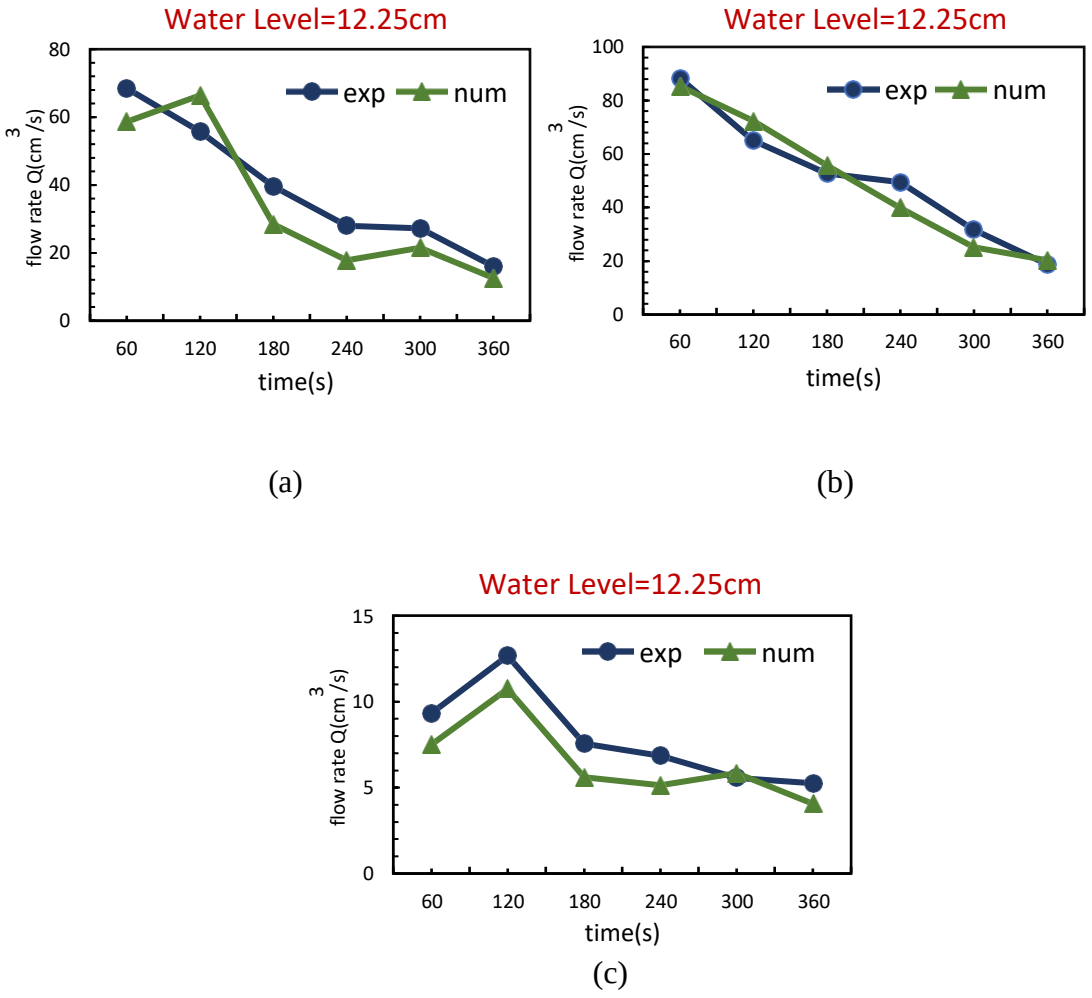

Fig. 23. Flow rate (frequency-1.75 Hz and water level- 12.25 cm) for three different shapes (a) plain slope (b) converging slope, (c) stairs slope.

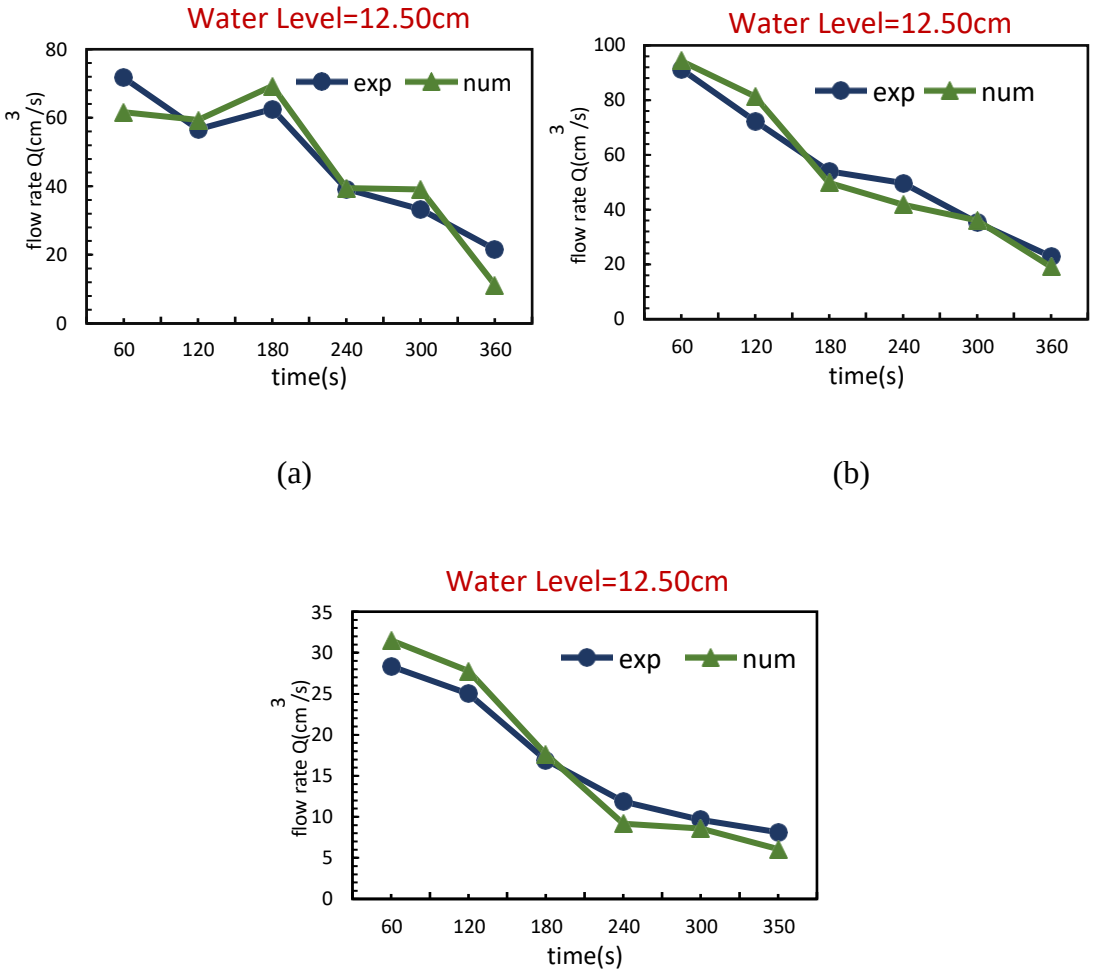

Fig. 24. Flow rate (frequency-1.75 Hz and water level- 12.50 cm) for three different shapes (a) plain slope (b) converging slope, (c) stairs slope.

The behaviour of overtopping structures for different frequencies has been plotted in a single graph in Fig. 25. As exhibited in the graph, stair slopes have much lower flowrate for every frequency compared to the other shapes, plain slopes have intermediate, whereas converging slopes have the highest flow rate for all frequencies. Fig. 26. shows a similar trend when total flowrate was plotted against water level. The flowrate

increases with water level height; but the effect is more significant for stair slope and plain slopes.

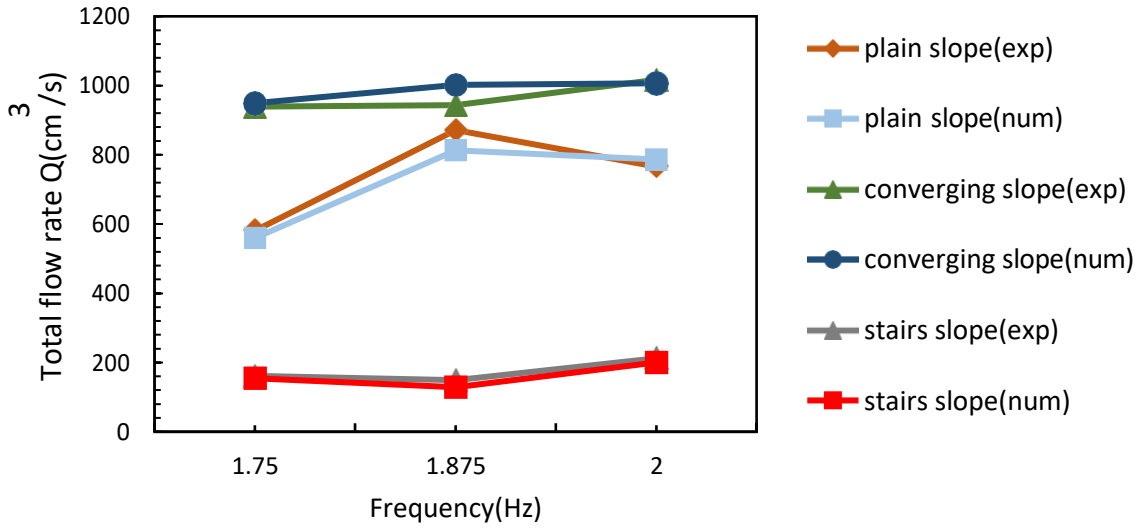

Fig. 25. Comparison of three different shapes between experimental and numerical results for total flow rates versus frequency

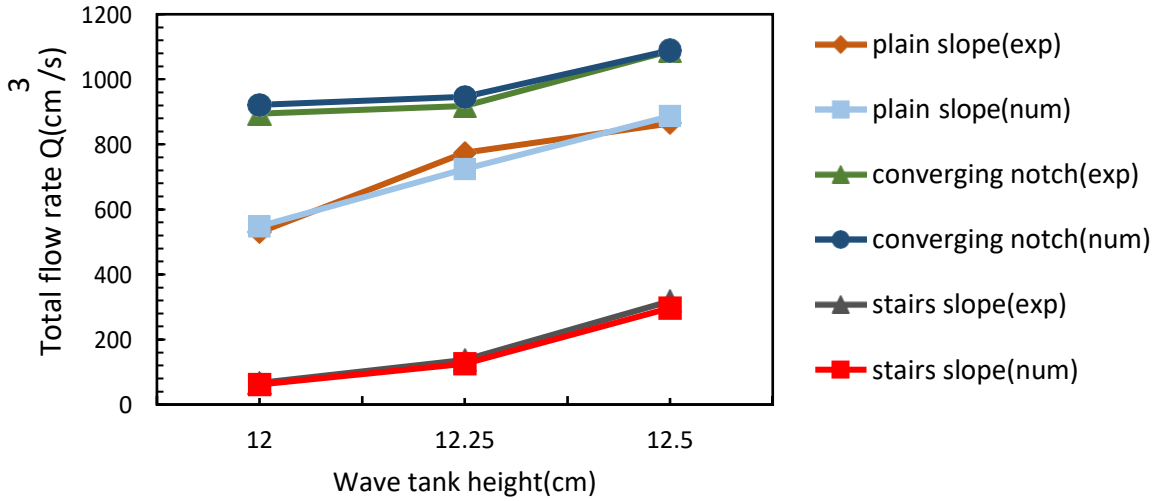

Fig. 26. Comparison of three different shapes between experimental and numerical results for total flow rates versus water level.

CHAPTER 6:

6. Conclusion

In recent years, wave energy converters are gaining popularity for harvesting wave energy and the search for the most efficient system still continues. To account for economic research, numerical wave tanks are used widely for which choosing the most suitable CFD code is crucial. For modelling numerical wave tanks, Flow-3D has been used extensively among a lot of other CFD codes. The simulations have been carried out using Reynolds Averaged Navier-stokes equation coupled with a volume-of-fluid model.

The goal of the present study is to investigate through experiments and numerical models the performance of different overtopping structures in producing overtopping discharges. Even though plain slopes have gained much acceptance by varying slope angle and optimizing the best angle for overtopping, this study shows that converging slopes do a much better job than plain slopes. It is found that numerical results are in reasonable agreement with experimental ones. A minor difference is present which can be ignored since they are due to experimental limitations and difficulties in explaining the real situation numerically. By finding a balance between accuracy and computational time, a perfect grid size has been curated for conducting all the tests through a mesh sensitivity analysis.

The experiments have been conducted numerically and the dimensions and parameters of the numerical wave tank is exactly the same as the experimental one. The wave patterns generated by the NWT matched the experiment exactly and thus serves as a virtual wave tank. This enables numerical models to be used to simulate wave tanks of

such features that are beyond the capabilities of laboratory experiments, helping to build prototypes. To further the cause of figuring out the best shape, pressure contour profiles have been added. It shows reasonably well the wave parameters and the effects of different overtopping structures on the wave overtopping process. These detailed information are valuable and will prove to be crucial for advanced design of Overtopping Breakwater for Energy Conversion (OBREC) in the future.

Nomenclatures

$\vec{V}_G$	velocity of mass center	$\vec{T}_{ni}$	Non-inertia torque
ω	angular velocity	m	Rigid body's mass
F	Total Force	r	Density of the fluid
T_G	Total torque about G	u	Fluid velocity
$[J]$	Moment of inertia tensor about G	V_f	Volume fraction
$\vec{F}_g$	Gravitational force	A_f	Area fraction
$\vec{F}_h$	Hydraulic force	p	pressure
$\vec{F}_c$	Net control force	τ	Viscous stress tensor
$\vec{F}_{ni}$	Non-inertia force	G	Gravity
$\vec{T}_g$	Gravitational torque	F_f	Fluid fraction
$\vec{T}_h$	Hydraulic torque	ρ	Fluid density

Abbreviations:

exp	Experiment
num	Numerical
OWEC	overtopping wave energy converter
WEC	Wave energy converter

SPH	Smoothed Particle Hydrodynamics
NWT	Numerical wave tank
VOF	Volume of Fluid
GMO	General moving object

Reference

[1] T. Aderinto and H. Li, "Ocean Wave energy converters: Status and challenges," *Energies*, vol. 11, no. 5, pp. 1–26, 2018, doi: 10.3390/en11051250.

[2] A. Uihlein and D. Magagna, "Wave and tidal current energy - A review of the current state of research beyond technology," *Renew. Sustain. Energy Rev.*, vol. 58, pp. 1070–1081, 2016, doi: 10.1016/j.rser.2015.12.284.

[3] W. M. (USA) John Huckerby (New Zealand), Kwang Soo Lee (Republic of Korea) and J. T.-M. (Cuba) Teresa Pontes (Portugal), "Lewis, A., S. Estefen, J. Huckerby, W. Musial, T. Pontes, J. Torres-Martinez, 2011: Ocean Energy. In IPCC Special Report on Renewable Energy Sources and Climate Change Mitigation [O. Edenhofer, R. Pichs-Madruga, Y. Sokona, K. Seyboth, P. Matschoss, S. Kad."

[4] G. Mørk, S. Barstow, A. Kabuth, and M. T. Pontes, "Assessing the global wave energy potential," *Proc. Int. Conf. Offshore Mech. Arct. Eng. - OMAE*, vol. 3, no. 2008, pp. 447–454, 2010, doi: 10.1115/OMAE2010-20473.

[5] Z. Han, Z. Liu, and H. Shi, "Numerical study on overtopping performance of a multi-level breakwater for wave energy conversion," *Ocean Eng.*, vol. 150, no. October 2017, pp. 94–101, 2018, doi: 10.1016/j.oceaneng.2017.12.058.

[6] D. D. Prasad, M. R. Ahmed, Y. H. Lee, and R. N. Sharma, "Validation of a piston type wave-maker using Numerical Wave Tank," *Ocean Eng.*, vol. 131, no. November 2014, pp. 57–67, 2017, doi: 10.1016/j.oceaneng.2016.12.031.

[7] M. Anbarsooz, M. Passandideh-Fard, and M. Moghiman, "Fully nonlinear

viscous wave generation in numerical wave tanks," *Ocean Eng.*, vol. 59, pp. 73–85, 2013, doi: 10.1016/j.oceaneng.2012.11.011.

[8] J. F. M. Gadelho, A. Lavrov, C. Guedes Soares, R. Urbina, M. P. Cameron, and K. P. Thiagarajan, "CFD modelling of the waves generated by a wedge-shaped wave maker," *Marit. Technol. Eng. - Proc. MARTECH 2014 2nd Int. Conf. Marit. Technol. Eng.*, vol. 2, no. 5, pp. 993–1000, 2015, doi: 10.1201/b17494-133.

[9] F. M. Marques Machado, A. M. Gameiro Lopes, and A. D. Ferreira, "Numerical simulation of regular waves: Optimization of a numerical wave tank," *Ocean Eng.*, vol. 170, no. May, pp. 89–99, 2018, doi: 10.1016/j.oceaneng.2018.10.002.

[10] M. H. Dao, L. W. Chew, and Y. Zhang, "Modelling physical wave tank with flap paddle and porous beach in OpenFOAM," *Ocean Eng.*, vol. 154, no. February, pp. 204–215, 2018, doi: 10.1016/j.oceaneng.2018.02.024.

[11] S. Shao, "Incrompressible SPH simulation of wave breaking and overtopping with turbulence modelling," *Int. J. Numer. Methods Fluids*, vol. 50, no. 5, pp. 597–621, 2006, doi: 10.1002/fld.1068.

[12] D. Vicinanza, P. Contestabile, J. Quvang Harck Nørgaard, and T. Lykke Andersen, "Innovative rubble mound breakwaters for overtopping wave energy conversion," *Coast. Eng.*, vol. 88, pp. 154–170, 2014, doi: 10.1016/j.coastaleng.2014.02.004.

[13] D. Vicinanza, J. H. Nørgaard, P. Contestabile, and T. L. Andersen, "Wave loadings acting on Overtopping Breakwater for Energy Conversion," *J. Coast.*

Res., vol. 65, no. SPEC. ISSUE 65, pp. 1669–1674, 2013, doi: 10.2112/SI65-282.1.

[14] A. Y. Maliki, M. A. Musa, M. F. Ahmad, I. Zamri, and Y. Omar, "Comparison of numerical and experimental results for overtopping discharge of the obrec wave energy converter," *J. Eng. Sci. Technol.*, vol. 12, no. 5, pp. 1337–1353, 2017.

[15] M. A. Musa, A. Y. Maliki, M. F. Ahmad, W. N. Sani, O. Yaakob, and K. B. Samo, "Numerical simulation of wave flow over the overtopping breakwater for energy conversion (OBREC) device," *Procedia Eng.*, vol. 194, pp. 166–173, 2017, doi: 10.1016/j.proeng.2017.08.131.

[16] Z. Liu, Z. Han, H. Shi, and W. Yang, "Experimental study on multi-level overtopping wave energy convertor under regular wave conditions," *Int. J. Nav. Archit. Ocean Eng.*, vol. 10, no. 5, pp. 651–659, 2018, doi: 10.1016/j.ijnaoe.2017.10.004.

[17] M. Davanipour, H. Javanmardi, and N. Goodarzi, "Chaotic Self-Tuning PID Controller Based on Fuzzy Wavelet Neural Network Model," *Iran. J. Sci. Technol. - Trans. Electr. Eng.*, vol. 42, no. 3, pp. 357–366, 2018, doi: 10.1007/s40998-018-0069-1.

[18] K. Khalifehei, G. Azizyan, and C. Gualtieri, "Analyzing the performance ofwave-energy generator systems (SSG) for the Southern Coasts of Iran, in the Persian Gulf and Oman Sea," *Energies*, vol. 11, no. 11, 2018, doi: 10.3390/en11113209.

[19] M. A. Bhinder, C. G. Mingham, D. M. Causon, M. T. Rahmati, G. A. Aggidis, and R. V. Chaplin, “A joint numerical and experimental study of asurging point absorbing wave energy converter (WRASPA),” *Proc. Int. Conf. Offshore Mech. Arct. Eng. - OMAE*, vol. 4, no. PART B, pp. 869–875, 2009, doi: 10.1115/OMAE2009-79392.

[20] J. Reveillon, C. Pera, and Z. Bouali, “Examples of the potential of DNS for the understanding of reactive multiphase flows,” *Int. J. Spray Combust. Dyn.*, vol. 3, no. 1, pp. 63–92, 2011, doi: 10.1260/1756-8277.3.1.63.

[21] A. Babajani, “Hydrodynamic Performance of a Novel Ocean Wave Energy Converter,” vol. 8, no. 3, pp. 73–83, 2018, doi: 10.5923/j.ajfd.20180803.01.

[22] A. Babajani, M. Jafari, P. Hafezisefat, M. Mirhosseini, A. Rezania, and L. Rosendahl, “Parametric study of a wave energy converter (Searaser) for Caspian Sea,” *Energy Procedia*, vol. 147, pp. 334–342, 2018, doi: 10.1016/j.egypro.2018.07.101.

[23] A. A. Babajani, M. Jafari, and P. Hafezi Sefat, “Numerical investigation of distance effect between two Searasers for hydrodynamic performance,” *Alexandria Eng. J.*, vol. 55, no. 3, pp. 2257–2268, 2016, doi: 10.1016/j.aej.2016.05.022.